Generalized Inverse of a Reduced Gravity Primitive Equation Ocean Model and Tropical Atmosphere–Ocean Data

HANS E. NGODOCK, BOON S. CHUA, AND ANDREW F. BENNETT

College of Oceanic and Atmospheric Sciences, Oregon State University, Corvallis, Oregon

(Manuscript received 15 April 1999, in final form 2 September 1999)

ABSTRACT

A nonlinear 2½-layer reduced gravity primitive equations (PE) ocean model is used to assimilate sea surface temperature (SST) data from the Tropical Atmosphere–Ocean (TAO) moored buoys in the tropical Pacific. The aim of this project is to hindcast cool and warm events of this part of the ocean, on seasonal to interannual timescales.

The work extends that of Bennett et al., who used a modified Zebiak–Cane coupled model. They were able to fit a year of 30-day averaged TAO data to within measurement errors, albeit with significant initial and dynamical residuals. They assumed a 100-day decorrelation timescale for the dynamical residuals. This long timescale for the residuals reflects the neglect of resolvable processes in the intermediate coupled model, such as horizontal advection of momentum. However, the residuals in the nonlinear PE model should be relatively short timescale errors in parameterizations. The scales for these residuals are crudely estimated from the upper ocean turbulence studies of Peters et al. and Moum.

The assimilation is performed by minimizing a weighted least squares functional expressing the misfits to the data and to the model throughout the tropical Pacific and for 18 months. It is known that the minimum lies in the ''data subspace'' of the state or solution space. The minimum is therefore sought in the data subspace, by using the representer method to solve the Euler–Lagrange (EL) system. Although the vector space decomposition and solution method assume a linear EL system, the concept and technique are applied to the nonlinear EL system (resulting from the nonlinear PE model), by iterating with linear approximations to the nonlinear EL system. As a first step, the authors verify that sequences of solutions of linear iterates of the forward PE model do converge. The assimilation is also used as a significance test of the hypothesized means and covariances of the errors in the initial conditions, dynamics, and data. A ''strong constraint'' inverse solution is computed. However, it is outperformed by the ''weak constraint'' inverse.

A cross validation by withheld data is presented, as well as an inversion with the model forced by the Florida State University winds, in place of a climatological wind forcing used in the former inversions.

1. Introduction

In the last two decades, an increasing interest in the study of ocean general circulation and its role in climate processes has led to improved data acquisition and to improved ocean models. A set of measurements is generally sparse in space and time, and cannot resolve the circulation and the physical scales of interest. On the other hand, a dynamical model contains information only about the interaction of the physical processes taken into account in the equations, and the model solutions are computed given a prior estimation of the initial and boundary conditions and the forcing. In general, outputs from a direct or forward run of the model do not fit the measurements. Thus, to find a good estimate of the actual state of the ocean, it is necessary to use all available information: the model and the measurements. Therefore, data assimilation methods become inevitable. These methods enable one to combine the information about the actual state of the ocean, contained in a set of measurements, with the other information about the dynamical processes of the ocean, given by a mathematical model. This approach can be considered as interpolating or smoothing the set of measurements in space and time, with the model acting as a dynamical constraint. The resulting estimate of the actual state of the ocean, also referred to here as the generalized inverse, should therefore be much more uniformly realistic than the estimates obtained from the measurements or the model alone.

Our assimilation method will consist of minimizing a weighted least squares functional expressing the model misfit to the data. The forcing is poorly known, numerically resolvable dynamics are sometimes neglected, unresolved dynamics are poorly parameterized; and truncation error especially in the vertical can be severe.

Corresponding author address: Dr. H. Ngodock, College of Oceanic and Atmospheric Sciences, Oregon State University, 104 Ocean Admin. Bldg., Corvallis, OR 97331-5503.
E-mail: ngodock@oce.orst.edu

Hence, we will only allow the model to act as a ''weak constraint'' (Sasaki 1970), contrary to the strong constraint approach that assumes the model to be perfect. Thus the functional shall, in addition to data and initial misfits, also contain terms that penalize the dynamical misfits.

The generalized inverse or the best fit may be obtained using variational methods. These lead to an Euler–Lagrange (EL) system, which in turn is solved using the representer method (Bennett 1992; Bennett et al. 1996). As described in these references, the generalized inverse is expressed as a first guess plus a finite linear combination of representer functions. The approach is based on the assumption that the forward model and the measurement operator or functional are linear.

The use of a primitive equation (PE) model on one hand offers the advantage of including the resolvable processes neglected by intermediate models. On the other hand, as with the intermediate models, it leads to a nonlinear EL system and thus prevents us from using the representers expansion immediately. We overcome this difficulty by solving the nonlinear EL equations iteratively. We devise linear iterates of the nonlinear EL equations. The iterates will be solved in turn by the representer method. We hope that the solution iterates converges; if it does, it will be to a solution of the nonlinear EL problem.

Solving a nonlinear EL system iteratively has already been implemented by Bennett and Thorburn (1992) for a nonlinear quasigeostrophic ocean model, by Bennett et al. (1996) for a global NWP model, and by Bennett et al. (1998) for an intermediate coupled model. We introduce a slight modification of their approach in order to avoid the difficulties they faced with their linearization. The basic requirement guiding any linearization is that the sequence of solutions of the linear approximate EL systems should converge toward the solution of the nonlinear EL system. In the case where there is no data, this method reduces to solving the nonlinear PE model iteratively: the subsequent sequence of solutions of the linear approximate PE models should converge toward the solution of the nonlinear PE model. We refer to these as the dataless iterations. Since there is no theoretical guarantee for convergence of the linear approximations of the full EL system, we will cautiously focus first on the dataless iterations. These preliminary calculations will be reported here. Then we will include the data and present the results of a generalized inversion with monthly mean Tropical Atmosphere–Ocean (TAO) SST data for December 1996–May 1998, containing the latest strong El Niño–Southern Oscillation (ENSO).

This paper is organized as follows: the model ocean is presented in section 2. The generalized inversion is presented in section 3, based on the iterated indirect representer method. The dataless iterations are presented in section 4, and the first inversion experiment in section 5. In section 6 we present a second inversion, which is a cross validation. A third inversion, with Florida State University (FSU) real-time winds in place of Rasmusson and Carpenter climatological winds (in the previous inversions), is presented in section 7. Then a summary and concluding remarks are presented in section 8.

2. The model ocean

We use a 2½-layer reduced-gravity PE ocean model, following McCreary and Yu (1992). We make a slight modification to the vertical discretization of the vertical advection terms: we use a centered differencing instead of the first-order upwind scheme, since the latter adds further nonlinearities and nondifferentiabilities to the discrete model operator. Details may be found in the appendix. We also replaced their biharmonic friction by a Laplacian friction, in the interest of simplicity. The equations of momentum, energy, and continuity are written in advective form as follows:

$$\frac{\partial \mathbf{v}_i}{\partial t} + \mathbf{v}_i \cdot \boldsymbol{\nabla}\mathbf{v}_i + f\mathbf{k} \times \mathbf{v}_i + \boldsymbol{\nabla} p_i = \delta_{1_i}\frac{\boldsymbol{\tau}}{h_1} - (\delta_{1_i} w_e + \delta_{2_i} w_d)\frac{(\mathbf{v}_1 - \mathbf{v}_2)}{h_i} + \kappa_2 \nabla^2 \mathbf{v}_i - \gamma \mathbf{i} u_i, \tag{1}$$

$$\frac{\partial T_i}{\partial t} + \mathbf{v}_i \cdot \boldsymbol{\nabla} T_i = \frac{Q_i}{h_i} - (\delta_{1_i} w_e + \delta_{2_i} w_d)\frac{(T_1 - T_2)}{h_i} + \kappa_2 \nabla^2 T_i, \tag{2}$$

$$\frac{\partial h_i}{\partial t} + \boldsymbol{\nabla} \cdot (h_i \mathbf{v}_i) = \varepsilon_i(\delta_{1_i} w_e + \delta_{2_i} w_d) + \kappa_2 \nabla^2 h_i, \tag{3}$$

where the index i stands for the layer; $\mathbf{v}$, h, and T denote the velocity, thickness, and temperature, respectively; $\boldsymbol{\tau}$ is the wind stress at the surface; Q_i is the heat added to layer i; $\mathbf{i}$ and $\mathbf{k}$ are the unit vectors in the east and vertical directions, respectively; δ_{ij} is the Kronecker delta; and $\varepsilon_i = -(-1)^i$. The equatorial β plane is adopted throughout, so that $f = \beta y$. A y-dependant drag coefficient $\gamma(y)$ is included in the zonal-momentum equations near the open northern and southern boundaries of the model ocean to prevent large-scale, boundary-trapped instability from developing there. The pressure gradient terms $\boldsymbol{\nabla} p_i$ are given by

$$\boldsymbol{\nabla} p_1 = \alpha g \boldsymbol{\nabla}[h_1(T_1 - T_3) + h_2(T_2 - T_3)] - \frac{1}{2}\alpha g h_1 \boldsymbol{\nabla} T_1 \quad \text{and} \tag{4}$$

$$\boldsymbol{\nabla} p_2 = \alpha g \boldsymbol{\nabla}[(h_1 + h_2)(T_2 - T_3)] - \alpha g\left(h_1 + \frac{1}{2}h_2\right)\boldsymbol{\nabla} T_2, \tag{5}$$

TABLE 1. Model parameters and descriptions.

Laplacian mixing coefficient	$\kappa_2 = 5 \times 10^3$ cm^2 s^{-1}
Maximum value of damper	$\gamma = 1$ day^{-1}
Surface heating timescale	$t_1 = 100$ day
Lower-layer heating timescale	$t_1 = 500$ day
Entrainment timescale	$t_e = 5$ day
Detrainment timescale	$t_d = 40$ day
Entrainment depth	$H_e = 75$ m
Detrainment depth	$H_d = 75$ m
Intial thickness of upper layer	$H_1 = 75$ m
Intial thickness of lower layer	$H_2 = 175$ m
Initial temperature of upper layer	$T_1^* = 28$°C
Intial temperature of lower layer	$T_2^* = 15$°C
Temperature of deep ocean	$T_3 = 0$°C
Coefficient of thermal expansion	$\alpha = 0.00025$°C^{-1}
Characteristic speed of mode 1	$c_1 = 316$ cm s^{-1}
Characteristic speed of mode 2	$c_2 = 123$ cm s^{-1}

where α is the (constant) coefficient of thermal expansion, g is the acceleration of gravity, and T_3 is the temperature of the deep ocean. The vertical velocities w_e (*entrainment*) and w_d (*detrainment*) are parameterized by

$$w_e = \frac{(H_e - h_1)^2}{H_e t_e}\Theta(H_e - h_1) \quad \text{and} \tag{6}$$

$$w_d = -\frac{(H_d - h_1)^2}{H_d t_d}\Theta(h_1 - H_d), \tag{7}$$

where $\Theta(x)$ is the Heaviside step function [$\Theta(x) = 1$ if $x > 0$, $=0$ otherwise]. According to this parameterization, entrainment occurs when the thickness of the upper layer is less than a specified constant value H_e, and its rate increases parabolically to a maximum value H_e/t_e as h_1 goes to zero. Similarly, detrainment occurs when the thickness of the upper layer becomes larger than H_d. Entrainment is a crucial process in this model, acting to prevent the interface from surfacing, to cool the upper layer, and to provide the stress between the two layers. Likewise, detrainment is important because only with detrainment can the model adjust to a reasonable mean state. In our computations $H_e = H_d$.

Finally, the heat fluxes are parameterized as follows:

$$Q_1 = \frac{H_1}{t_1}(T_1^* - T_1) \quad \text{and} \tag{8}$$

$$Q_2 = \frac{H_2}{t_2}(T_2^* - T_2). \tag{9}$$

Here T_1^* and T_2^* are the initial uniform temperatures of the layers, and t_1 and t_2 are timescales for the temperatures to relax back to the initial values. The heating Q_2 represents adjustment to a steady thermohaline circulation, and is necessary to balance the warming of the lower layer caused by detrainment. The constants α, g, H_e, H_1, H_2, t_e, t_1, t_2, T_1^*, T_2^*, and T_3 follow Table 1 of McCreary and Yu (1992) and are reproduced here in Table 1. All the parameterizations in (4)–(9) also follow that same reference. The model is forced by the climatological wind fields of Rasmusson and Carpenter (1982) for the dataless iterations (section 4) and the first two inversions (sections 5 and 6). For the third inversion, the climatological winds are replaced by FSU winds. We compute the model solutions in a rectangular basin of the tropical Pacific extending from 29°S to 29°N and 123.75°E to 84.52°W; eastern and western boundaries are closed, while a free slip condition is imposed at the northern and southern boundaries. The horizontal grid is stretched in such a way that the meridional grid spacing is about 0.3° near the equator and gradually increases to 1.3° at the northern and southern boundaries. The zonal grid spacing is about 0.3° near the eastern and western boundaries (to resolve the boundary layer) and gradually increases to about 2° in the middle of the ocean.

3. The generalized inversion

a. The Euler–Lagrange system

As mentioned in the introduction, we cannot apply the representer method directly in order to solve a nonlinear EL system. In this section, we describe how we circumvent the difficulty. We linearize the EL system around a given background field and solve the resulting linear EL system by the representer method. Then the solution of the linear EL becomes the background field for the next linearization and we iterate until apparent convergence. In solving iteratively the nonlinear EL equations, two approaches can be considered: 1) linearize directly the nonlinear EL equations, or 2) linearize the nonlinear forward model, and then derive the corresponding EL equations. In both cases, the linear approximations have to satisfy the following condition: (i) formal convergence toward the nonlinear problem at the limit. Note that by convergence we do not mean that of a numerical scheme of ever finer resolution, but rather that of a sequence of solutions of linear EL systems with fixed numerical resolution. Another condition that is effective but not necessary is (ii) that a linear EL problem be solved at each iterate, that is, the linearized EL equation has adjoint symmetry with respect to the linearized forward model. This condition enables the representer method, in the sense that it ensures the symmetry of the representer matrix. By construction, the symmetry of the representer matrix depends on two factors (Bennett 1992, chapter 5, section 5.4): the adjoint symmetry of the EL system, and the symmetry of the model (dynamical) error covariances. The latter are symmetric by definition and by choice, being covariances. Thus the symmetry of the representer matrix depends solely on the adjoint symmetry of the EL system. Therefore one has to preserve this symmetry carefully, when linearizing the EL system. This is achieved by following point 2 above and is described below. A fail-

ure to satisfy condition ii would worsen the conditioning of the solution process at each iterate.

To avoid the complexity of the model equations, we describe the linear iteration scheme using a simple nonlinear model. Consider the equation

$$u_t + \mathcal{F}(u)u_x = F + f,$$
$$0 \le t \le T, \qquad 0 \le x \le L, \tag{10}$$

where $F = F(x, t)$ is the prior estimate of model forcing, $f = f(x, t)$ is the residual or model error, while $\mathcal{F}$ is a prescribed nonlinear function of u. For the sake of simplicity, we assume homogeneous initial and boundary conditions. Given a vector of measurements: d_m, with errors $\boldsymbol{\epsilon}_m$,

$$d_m = u(x_m, t_m) + \boldsymbol{\epsilon}_m, \qquad 1 \le m \le M, \tag{11}$$

and prior estimates of the means and the covariances $C_f = C_f(x, t, x', t')$ and $\mathbf{C}_\epsilon$ for the model and observational errors, respectively, we can define a penalty functional:

$$J[u] = \int_0^T dt \int_0^T dt' \int_0^L dx \int_0^L dx' f(x, t)W_f(x, t, x', t') \times f(x', t') + \boldsymbol{\epsilon}^*\mathbf{W}_\epsilon\boldsymbol{\epsilon}, \tag{12}$$

where f is related to u as in (10), $\boldsymbol{\epsilon}_m$ to u as in (11), while W_f and $\mathbf{W}_\epsilon$ are the operator inverses of the covariances. We do not bother to include initial penalties in (12) for this discussion.

The fundamental assumption that allows us to use the variational approach for minimizing (12) is that $\mathcal{F}$ be differentiable, or at least Gâteaux differentiable (Milne 1980). We can then derive the EL system for a local extremum $\hat{u}$ of (12):

$$\hat{u}_t + \mathcal{F}(\hat{u})\hat{u}_x = F + C_f \bullet \mu, \quad \text{and} \tag{13}$$

$$-\mu_t - [\mathcal{F}(\hat{u})\mu]_x + \mathcal{F}'(\hat{u})\mu\hat{u}_x = \boldsymbol{\delta}^*\mathbf{W}_\epsilon(\mathbf{d} - \hat{\mathbf{u}}), \tag{14}$$

where $\boldsymbol{\delta}$ and $\hat{\mathbf{u}}$ are the vectors with components $\delta(x - x_m)\delta(t - t_m)$ and $\hat{u}(x_m, t_m)$, respectively, while $C_f \bullet \mu$ is defined by

$$C_f \bullet \mu(x, t) = \int_0^T dt' \int_0^L dx' C_f(x, t, x', t')\mu(x', t'). \tag{15}$$

We can meet the Gâteaux differentiability requirement for the nonlinear PE model operator with the modifications described in the appendix, if the layer thicknesses do not vanish.

b. Linear approximations

Our first attempt to linearize the EL system follows Bennett et al. (1996) and consists of linearizing directly the nonlinear EL system by rewriting (13) and (14) as

$$\hat{u}^n_t + \mathcal{F}(\hat{u}^{n-1})\hat{u}^n_x = F + C_f \bullet \mu^n \quad \text{and} \tag{16}$$

$$-\mu^n_t - [\mathcal{F}(\hat{u}^{n-1})\mu^n]_x = -\mathcal{F}'(\hat{u}^{n-1})\mu^{n-1}\hat{u}^{n-1}_x + \boldsymbol{\delta}^*\mathbf{W}_\epsilon(\mathbf{d} - \hat{\mathbf{u}}^n), \tag{17}$$

subject to linear homogeneous boundary, initial, and final conditions. This system is linear and formally consistent with (13) and (14) as $n \to +\infty$. Note that the linearized system has adjoint symmetry: it is equivalent to the EL system for a linear inverse. The first term in the rhs of (17) is included in order to satisfy our condition i. In a PE model, many such terms arise from the nonlinear advection, from the entrainment, and from the pressure gradient. However these inhomogeneous terms require the computation of a first guess for the adjoint equation, and they cause the iterative scheme to require the storage of both the time-dependent state and the time-dependent adjoint variables. Without the first inhomogeneous terms in (17), the system (16) and (17) is still a linear EL system for each n. But as $n \to +\infty$, it fails to be an EL system and so its solutions formally fail to converge toward the solution of the nonlinear EL system (13) and (14).

We propose below another linearization that will satisfy both our conditions i and ii simultaneously, without adding any inhomogeneous terms. This second approach consists of linearizing the forward model first, then deriving the associated EL equation. We will see that if the nonlinearities in the forward model are ''properly'' treated (linearized), then by taking the adjoint, not only do we (automatically) meet the adjoint symmetry requirement for the linearized EL system, but we also ensure its consistency and convergence toward the nonlinear EL system. Given a ''good'' starting point field $\hat{u}^o$, we assume that the difference between two consecutive iterated solutions of the linearized forward model is small. Therefore, we can linearize the forward model as a first-order Taylor expansion around the previous iterate. Hence, we approximate (10) by the tangent linearization (see Lacarra and Talagrand 1988):

$$u^n_t + \mathcal{F}(\hat{u}^{n-1})u^n_x + \mathcal{F}'(\hat{u}^{n-1})(u^n - \hat{u}^{n-1})\hat{u}^{n-1}_x = F + f. \tag{18}$$

Compared to (16), the additional term in the left-hand side can be thought of as a correction term. The EL system corresponding to this linearization is

$$\hat{u}^n_t + \mathcal{F}(\hat{u}^{n-1})\hat{u}^n_x + \mathcal{F}'(\hat{u}^{n-1})(\hat{u}^n - \hat{u}^{n-1})\hat{u}^{n-1}_x = F + C_f \bullet \mu^n \quad \text{and} \tag{19}$$

$$-\mu^n_t - [\mathcal{F}(\hat{u}^{n-1})\mu^n]_x + \mathcal{F}'(\hat{u}^{n-1})\hat{u}^{n-1}_x\mu^n = \boldsymbol{\delta}^*\mathbf{W}_\epsilon(\mathbf{d} - \hat{\mathbf{u}}^n). \tag{20}$$

These equations are linear, they do compose an EL system, and they have no inhomogeneous terms as in (17). Moreover, as $n \to +\infty$, they converge toward the EL system associated with the nonlinear forward model.

With the linearization (19) and (20), we also avoid the storage of the time-dependent adjoint variable. However, we run the risk of introducing an additional linear instability into the linearized dynamics: compare the left-hand sides of (19) and (20), to those of (16) and (17).

c. Significance test

Generalized inversion is not only aimed at fitting the model to the data; it is also a test of the hypothesized prior statistics for the errors. If the model error f and the data error ϵ have zero means, and are uncorrelated (i.e., $\overline{f} = \overline{\epsilon} = \overline{f\epsilon} = 0$), and if f and ϵ are Gaussian with the prescribed covariances C_f and C_ϵ, then it may be demonstrated (Bennett 1992) for linear models that the reduced penalty functional is a χ^2 random variable with M degrees of freedom, where M is the number of measurements. This random variable has mean M and variance $2M$.

d. Estimating the scales for the model errors

The advantage of the McCreary and Yu primitive equations ocean model over the intermediate model considered by Bennett et al. (1998) is that the PE model includes all the resolvable processes such as momentum advection and mean advection of mean heat. Thus there are fewer sources of error in the PE model, even though those remaining sources are themselves significant. Faced with the confusion of estimating errors arising from the neglect of resolvable processes as well as unreliable parameterization of unresolved processes, Bennett et al. based their estimates of dynamical errors on the former alone. One of the most difficult aspects of developing priors is assigning correlation scales for model errors. At least in the case of neglected but resolvable processes, it can be reasonably assumed that the processes involve the El Niño disturbance itself, and so it is plausible that correlation scales are those of the disturbance itself. For the McCreary and Yu model, however, we can only attribute errors to the inadequacies of subgrid-scale parameterizations. Given the extreme crudity of the vertical resolution, we shall set aside the horizontal flux errors and only consider vertical flux errors. The upper-ocean turbulence studies of Moum (1996), Peters (1994), and the information in Fig. 10 of Peters et al. (1988) are particularly helpful. To begin, consider the momentum balance

$$\frac{\partial u}{\partial t} + \cdots = \cdots \rho^{-1}\frac{\partial}{\partial z}J_m, \tag{21}$$

where J_m is the vertical eddy flux of horizontal momentum. The variation of J_m in the first 50 m of the water column is about 0.05 N m^{-2}; thus, its vertical divergence is about 1×10^{-3} N m^{-3}. We assume that the parameterization of this eddy flux divergence as the entrainment formula in (1) is 100% in error for layer 1. With $\rho_i \cong 10^3$ kg m^{-3}, we arrive at a residual $r_u^{(1)}$ for (1) of 1×10^{-6} m s^{-2}. The flux divergence observed by Peters et al. (1988) and entrainment formula computed here have much smaller values in the lower layer so we assume $r_u^{(2)} = 1 \times 10^{-7}$ m s^{-2}.

TABLE 2. Standard deviations, length scale, and timescale for the model residuals.

Residuals	Std dev σ	Zonal scale	Meridional scale	Timescale
$r_u^{(1)}$, $r_v^{(1)}$	10^{-6} m s^{-2}	10^6 m	2.5×10^5 m	2×10^6 s
$r_u^{(2)}$, $r_v^{(2)}$	10^{-7} m s^{-2}	10^6 m	2.5×10^5 m	2×10^6 s
$r_T^{(1)}$	2.5×10^{-7} K s^{-1}	10^6 m	10^6 m	2×10^6 s
$r_T^{(2)}$	2.5×10^{-8} K s^{-1}	10^6 m	10^6 m	2×10^6 s
$r_h^{(1)}$	$\lvert w_e\rvert \sim 10^{-6}$ m s^{-1}	10^6 m	10^6 m	2×10^6 s
$r_h^{(2)}$	$\lvert w_e\rvert \sim 10^{-7}$ m s^{-1}	10^6 m	10^6 m	2×10^6 s

The heat balance is

$$\frac{\partial T}{\partial t} + \cdots = \cdots (\rho C_p)^{-1}\frac{\partial}{\partial z}J_h, \tag{22}$$

where J_h is the vertical eddy flux of heat. The variation of J_h in the first 50 m of the water column is about 50 W m^{-2}; thus, its vertical divergence is about 1 W m^{-3}. Again, we assume that the entrainment formula in (2) is 100% in error for layer 1. With $\rho C_p \cong 4 \times 10^6$ J m^{-3} K^{-1}, we arrive at a residual $r_T^{(1)}$ for (2) of 2.5×10^{-7} K s^{-1}. The value of $r_T^{(2)}$ is assumed to be 10 times smaller.

We have no data for vertical thickness fluxes so we assume that the computed entrainment values in (3) are 100% in error. That is, we estimate $r_h^{(1)}$ to be 10^{-6} m s^{-1}, with $r_h^{(2)}$ 10 times smaller.

There are no data for horizontal and temporal correlation scales for vertical fluxes. Moum et al. (1989) remark that the fluxes are influenced by the passage of 20-day tropical instability waves. It is plausible that the fluxes are so influenced over the 1000-km zonal wavelength of such waves. We therefore speculate that, even though the eddy fluxes are not due solely to the passage of the tropical instability waves, errors in flux parameterizations could also be correlated over scales of 20 days, 1000 km zonally, and 250 km across the meridional extent of the equatorial current system. These assumptions can scarcely be defended, yet we can find no contrary data nor even contrary arguments. It is emphasized that the process of inversion is a test of these assumptions with a model and a large-scale circulation data. Our scales are summarized in Table 2. Finally, the spatial and temporal forms of the covariances have the simple separable Gaussian forms in Bennett et al. (1998), except with the scales described above.

4. The dataless iterations

As stated above, there is no rigorous mathematical proof for the convergence of this iterative scheme, for fixed time intervals of arbitrary length. We can therefore speak of convergence only formally, when we seek a sequence of numerical solutions of system (19) and (20)

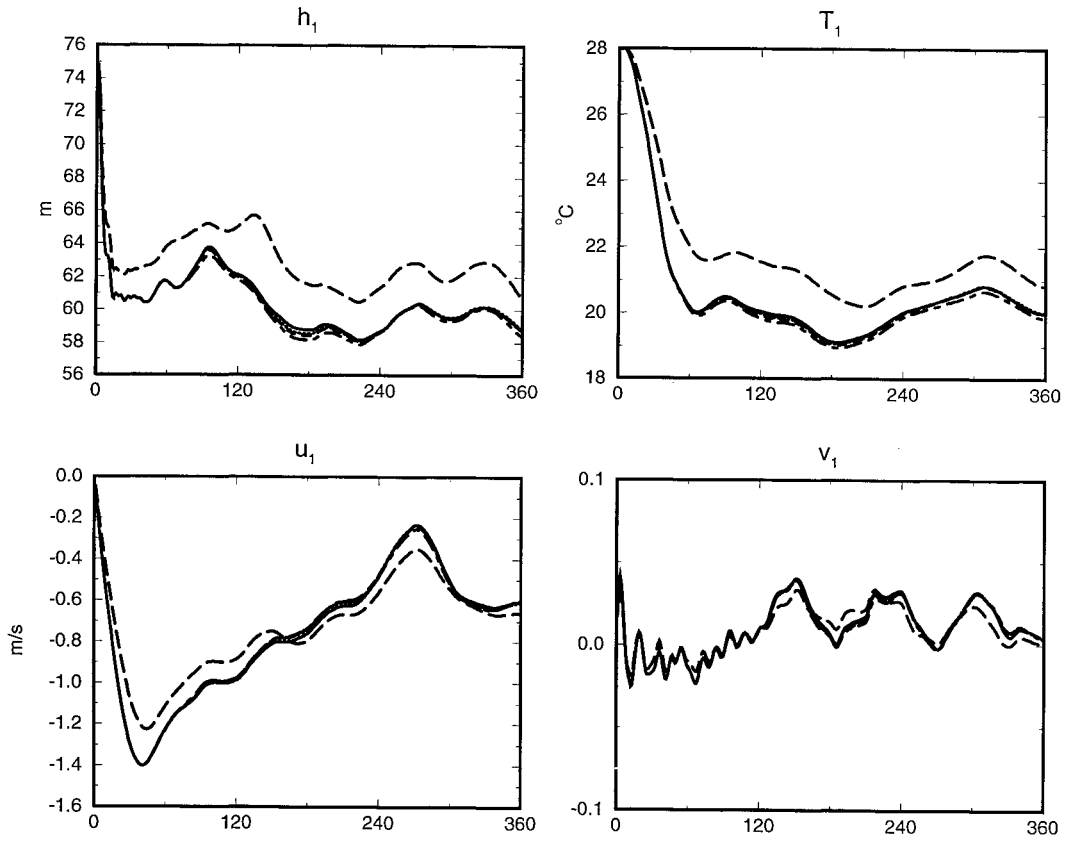

FIG. 1. Time series of the upper-layer model variables h, T, u, and v, picked at location (0°, 160°W), in the first experiment. The figure shows the nonlinear solution (solid line), the first guess $n = 0$ (long-dashed line), $n = 20$ (dotted–dashed line), $n = 30$ (dashed line), and $n = 39$ (dotted line).

converging toward the solution of system (13) and (14). There is a proof of convergence for the inverse of a barotropic vorticity equation by Hagelberg et al. (1996). Before implementing the iterations on the full nonlinear EL system, we will first seek to solve the nonlinear PE model iteratively. This corresponds to the case when there are no data at all, or the data are worthless ($\mathbf{W}_\epsilon = \mathbf{0}$). In this case, the linearized EL system (19) and (20) is reduced to

$$u_t^n + \mathcal{F}(u^{n-1})u_x^n + \mathcal{F}'(u^{n-1})(u^n - u^{n-1})u_x^{n-1} = F, \quad (23)$$

and we require its associated sequence of solutions to converge, as $n \to +\infty$, toward the solution of

$$u_t + \mathcal{F}(u)u_x = F. \quad (24)$$

Were this test to fail, there would be concern for the convergence of the iterations on the full problem, that is, with positively weighted data. Then again, we might speculate that data in fact ''guide'' the convergence.

We have applied the linearization (18) on the nonlinear PE model (1)–(9) and then iterated. The full linearized equations are given in the appendix. First we computed the solution of the nonlinear PE model forced by the climatological wind stress of Rasmusson and Carpenter (1982) for one year. This solution served as the reference solution toward which the iterated solutions should converge. We used, as the ''$n = 0$'' first guess for the iteration, a solution of the nonlinear PE model with the wind stress decreased by 20%. For $n \geq 1$, we restored the full wind stress. To explore robustness of the linearization, and to show that the convergence does not depend on this idealized first guess, we did a second experiment with a first guess computed using 50% of the wind stress. In the figures below (Figs. 1–4), we present time series of upper- and lower-layer thickness, temperature, zonal and meridional currents at (0°N, 160°W) for both experiments. Time series for many other locations were examined, and all show convergence toward the nonlinear solution in both experiments. We include only essential examples here. Each panel in Figs. 1–4 consists of the reference or nonlinear solution (solid line), the $n = 0$ first guess to start the iterations (long-dashed line), $n = 20$ (dotted–dashed line), $n = 30$ (dashed line), and $n = 39$ (dotted line). The figures display the convergence of all variables in both experiments.

Comments

We observed some oscillations in the sequence of iterations in preliminary computations (not shown), so

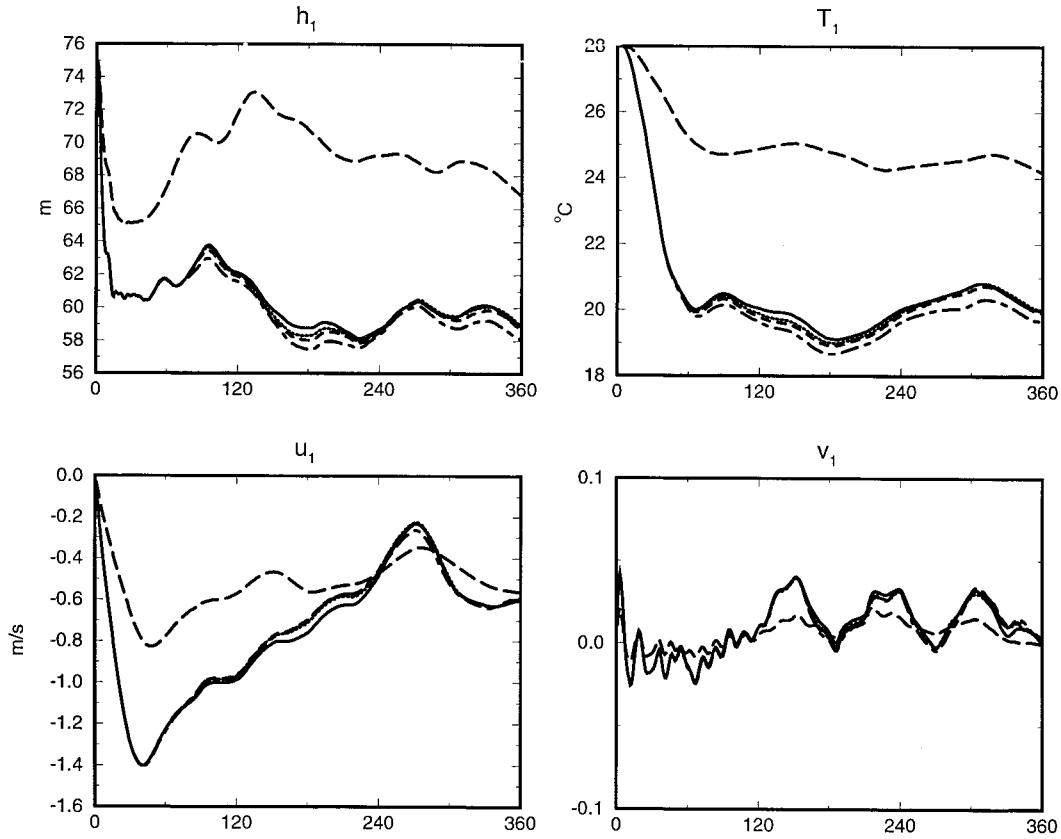

FIG. 2. Same as in Fig. 1 except for the second experiment.

we included a smoothing relaxation term $\nu\nabla^2(u^n - u^{n-1})$ in the rhs of (23), in order to damp these oscillations. This term vanishes formally as $n \to +\infty$. A large value of ν damps the oscillations and accelerates convergence, provided it does not break the numerical stability criterion. The smoothing relaxation term was included in every equation of the PE model, with $\nu = 7 \times 10^4$ m^2 s^{-1}.

In the first experiment (using 80% of the wind stress to compute the first guess), the time series of the upper- and lower-layer variables converged in about 20 iterations at all test locations, as shown in the panels of Figs. 1 and 3 for our display location (0°, 160°W). Note that the first guess in this experiment was not very far from the reference solution. Except for the initial condition, which is the same for all the iterates, the largest discrepancies between the first guess and the reference solution in the upper layer were about 1–3 m for h_1, about 1°–2°C for T_1, less than 20 cm s^{-1} for u_1, and only a few (1–2 cm s^{-1}) for v_1, at our display location. These discrepancies were about the same in the lower layer as in the upper layer, except for T_2 (less than 1°C). After 20 iterations all these discrepancies have almost vanished in both layers, and after 30 iterations, there is no difference between the iterated solution and the reference solution.

In the second experiment (50% of the wind stress), there were larger discrepancies between the reference solution and the first guess (Figs. 2 and 4), as one would expect. For example, in the upper layer, the dynamical discrepancy was about 6–12 m for h_1, 1°–5°C for T_1, and 10–60 cm s^{-1} for u_1. In the lower layer the discrepancies were about 4–15 m for h_2, 0.3°–1.5°C for T_2, and 10–60 cm s^{-1} for u_2. After 30 iterations, the upper-layer discrepancies were reduced to less than 40 cm for h_1, 0.5°C for T_1, 0.5 cm s^{-1} for u_1, and were about the same range for the lower-layer variables.

In both experiments, the iterated solutions converged toward a common limit. The second experiment needed more iterations than the first. Effective convergence was attained in about 30 iterations for both experiments, by which time the discrepancies are reduced to less than 10% of their initial values. The reduced discrepancies are then comparable to or smaller than the errors in the TAO data that will be introduced subsequently: see section 5 (fifth paragraph). Convergence proceeds from ''left to right'' in time, since all the iterates have the same initial conditions.

5. Experiments and results

The iterative inversion method described above (section 3) was applied to the nonlinear PE model in section

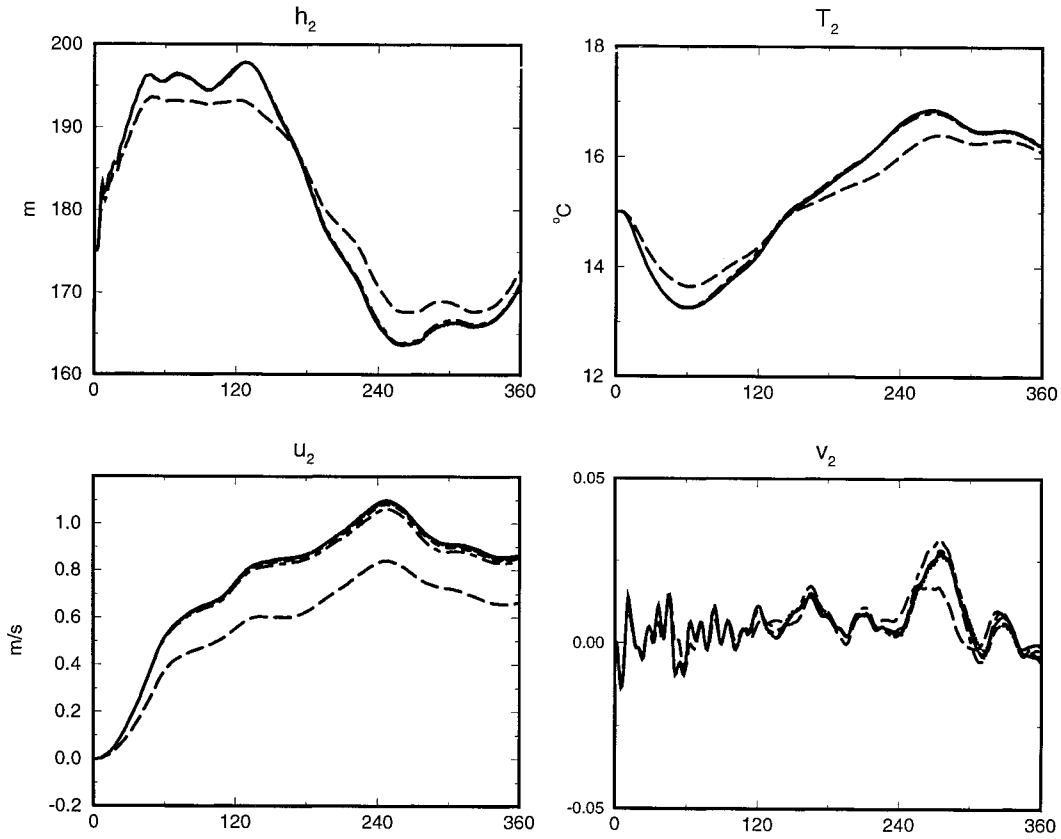

FIG. 3. Same as in Fig. 1 except for the lower layer.

2, for the assimilation of monthly mean sea surface temperatures data from the TAO buoys. The data cover a period of 18 months, from December 1996 to May 1998. This dataset consists of 1088 measurements (real numbers) and contains the latest strong ENSO signal, peaking in November–December 1997 with a 5°C anomalous warm pool in the eastern equatorial Pacific. TAO data are available from the Pacific Marine Environmental Laboratory (PMEL) via the Internet. The PMEL-distributed TAO display software provides gridded SST and 20°C isotherm depth (Z20) using an objective analysis procedure. We emphasize that we assimilated the TAO monthly mean SST at buoy locations. The gridded SSTs from PMEL/TAO software are only used for comparison with the inverse solution.

The first background field needed to start the linear iterations is generated by a direct run of the model with uniform initial conditions, forced by the climatological wind, and without either data or model error. This solution is labeled $n = 0$ in the figures on the assimilation. We linearize the nonlinear PE model around this background field and solve the associated linearized EL equations by the representer method. The solution of this linear inverse becomes the background field for the new linearization, and so on. Note that the climatological wind forcing is used in the dataless iterations, and this same climatological wind is used in the generalized inversion at each iterate.

The inverse shows ability to retrieve SST large-scale features as shown by the ''quick look'' maps from the PMEL TAO project (Figs. 5 and 6). The results presented in these figures, and also in Figs. 7 and 8, were obtained after five iterations. The inverse SST fields display more variability than PMEL maps. The latter are obtained by bilinear interpolation; thus, they do not contain dynamical interactions of physical processes. Subtracting the climatological SST monthly means (Rasmusson and Carpenter 1982) from the inverse SST fields, we get anomalous SST fields that are in good agreement with PMEL anomalous SST maps. The warm and cool pools are retrieved by the inverse, at the same locations as in PMEL maps, with slight differences in shape. For example, the maximum anomalous warming (5°C) occured in December 1997 along the equator, between 100° and 110°W, as shown on the TAO maps (Fig. 5b). The inverse solution shows an anomalous warm pool of 4.5°C at the same location (see Fig. 6b). In both figures, we can see that the anomalous temperature decreases westward, from 5°C (100°W along the equator) to 1°C (175°–170°W).

The generalized inverse tightly smoothes the data at the measurement locations and gives an estimate of the

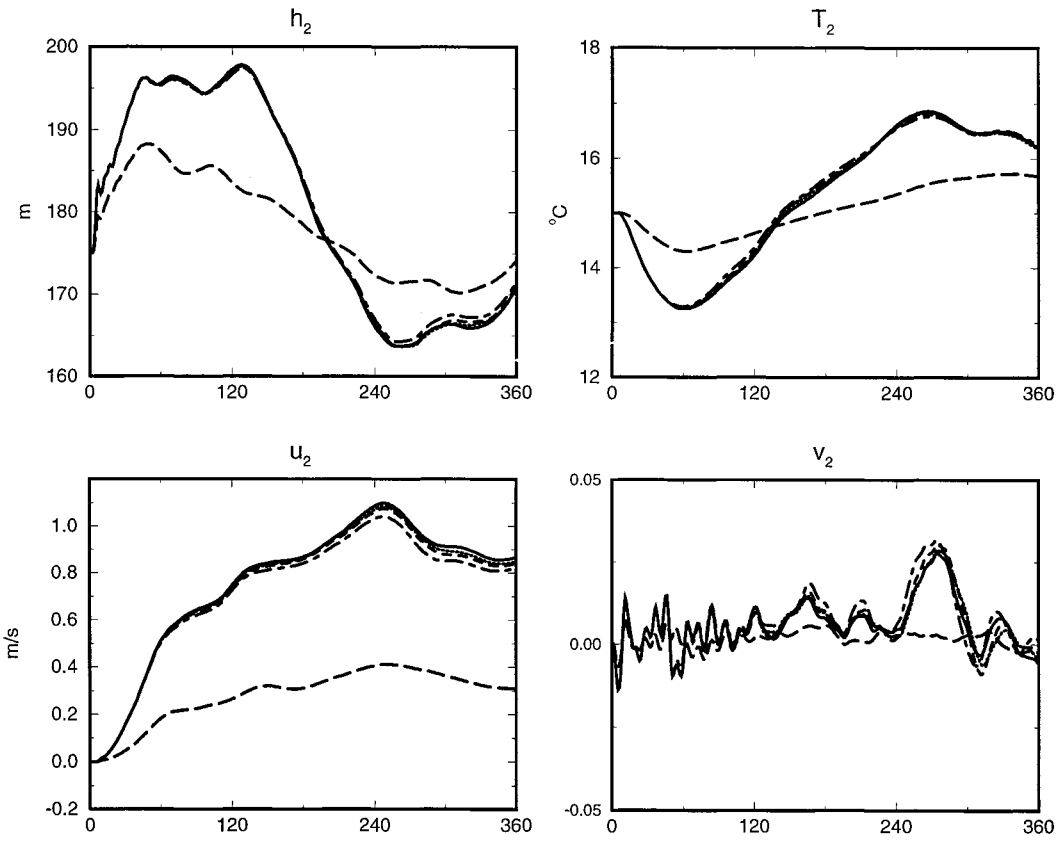

FIG. 4. Same as in Fig. 3 except for the second experiment.

circulation where and when the data are not available. This is best shown by the time series (Figs. 7–9). We show selected time series, along the equator (Fig. 7) and off the equator (Fig. 8). Although the background solution ($n = 0$) is far from the data (by as much as 8°C at some locations in Fig. 8), the inverse fits the data to within one standard measurement error, here 0.3°C for every single data. This data error accounts for the instrumental error (0.1°C), the interpolation from TAO buoy locations to neighboring model grid points (0.1°C), and the inconsistency of (linearly) relating temperatures measured at ocean levels to a layered model (0.1°C). Here we have the difficulty of identifying SST with the temperature in the model's 50-m-thick upper layer (M. McPhaden, PMEL/TAO Project Office, 1998, personal communication) The fit to the data is similarly good at all measurement sites. We also show in Fig. 9 an example of how the time series behave as we iterate. They are very close to each other for $n \geq 1$. Indeed, each iterate is a linear inverse solution that tries to fit the data. The situation is very much the same at all mooring locations. The main conclusion here is that complex fields governed by Rossby wave–like and Kelvin wave–like dynamics can be reconciled with the TAO data.

Because the data do not vary as we iterate, we can say that they ''guide'' the iterations, in the sense of fixed values. This explains why a small number of iterations (five) is needed for the generalized inverse to converge, compared to 30 in the dataless iterations (section 4).

The quality of our assimilation is not only assessed by the close fit to the data, but also by the reduced (minimal) value of the penalty functional $\hat{J}$, after we have performed the inversion. As stated above (section 3c), if the hypothesis about the prior means and covariances for the model and data errors is true, then $\hat{J}$ should be a χ^2 random variable with M degrees of freedom. For our iterative inversion, we expect the value of $\hat{J}$ at each iterate to be M (1088 in this experiment). The values of the prior and posterior (reduced) penalty functional are displayed in Fig. 10, showing that $\hat{J}$ ($\simeq$900) is about four standard deviations below the expected value, that is, 17% smaller than the mean. This hints that we were pessimistic about the scales and variances in section 3d. Remember that the mean of χ^2_M is M, and its standard deviation is $\sqrt{2M}$.

Also, Fig. 10 shows the different contributions to $\hat{J}$: posterior misfits for initials conditions, dynamics, and data. The prior penalty functional is only the misfit between the data and the first guess, since the first guess satisfies the dynamics, initial, and boundary conditions exactly. Clearly, $\hat{J}$ is largely dominated by the posterior dynamical misfits, compared to those for the initial con-

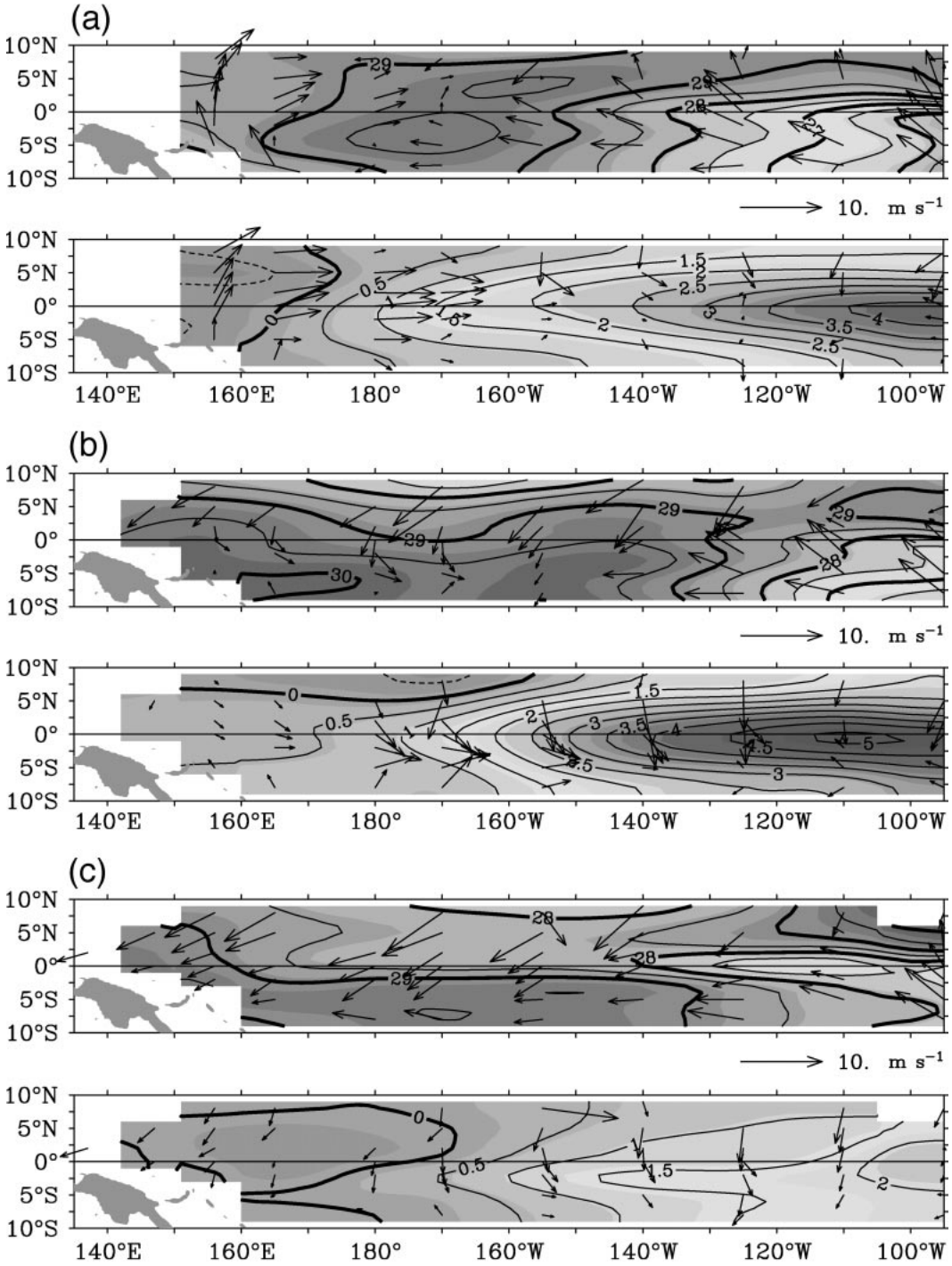

FIG. 5. Monthly means SST and SST anomalies from PMEL: (a) Aug 1997, (b) Dec 1997, and (c) May 1998.

ditions and the data. This suggests that the inversion could not be performed using the model as a strong constraint (no dynamical errors) when fitting the data. In fact, we ran an experiment with an assumption of no dynamical error ($C_f = 0$). The comparative fits at one mooring (0°, 95°W) are shown in Fig. 11, which confirms the suggestion. The shortcoming of the strong constraint experiment is due presumably to the long interval of time (18 months) for the assimilation. Initial conditions cannot control the ocean circulation beyond the model decorrelation timescale (about three months), which is about the time when the strong constraint solution loses track of the data.

Preliminary attempts to assimilate 20° and 16°C iso-

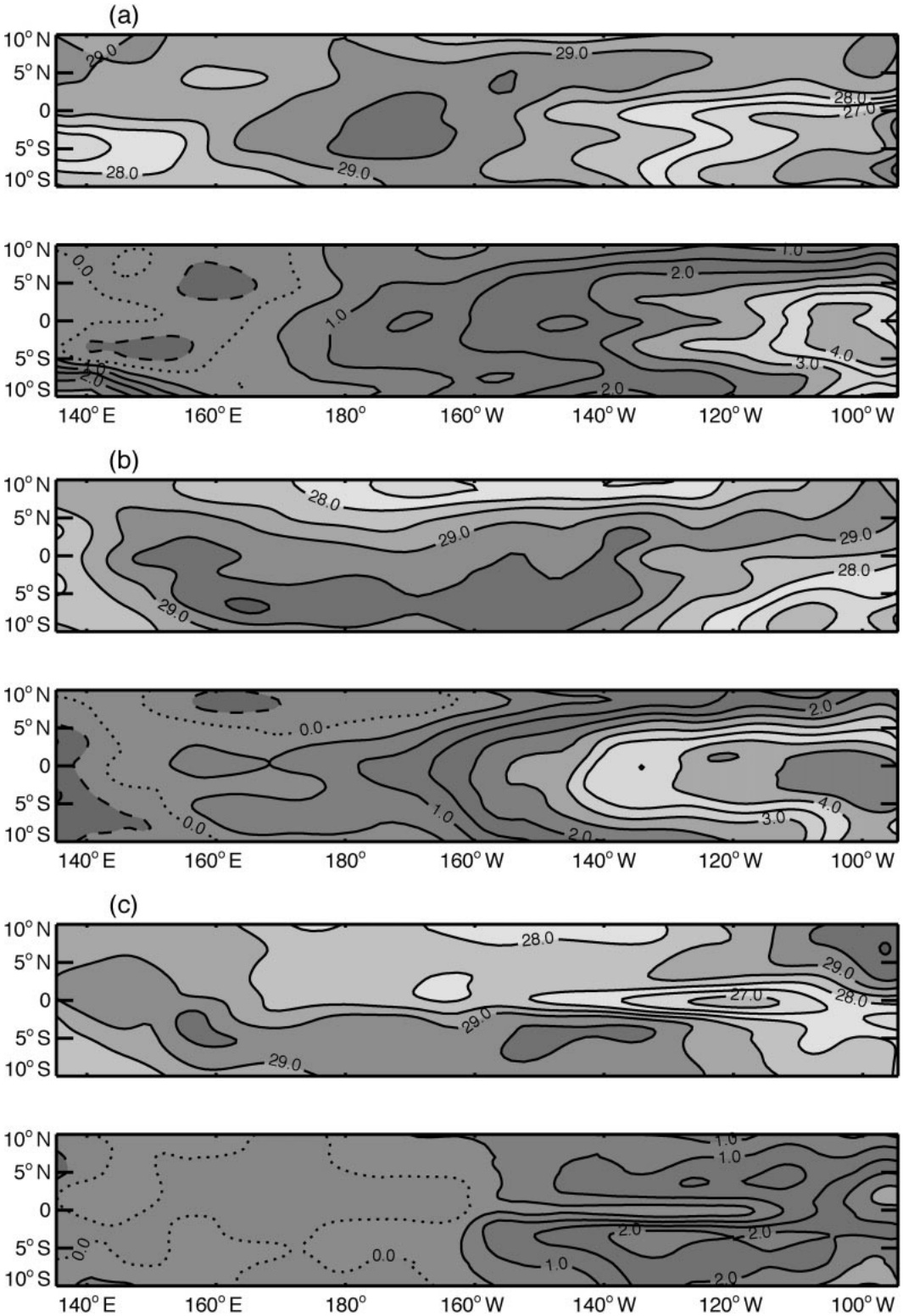

FIG. 6. Monthly means SST and SST anomalies from the generalized inverse: (a) Aug 1997, (b) Dec 1997, and (c) May 1998.

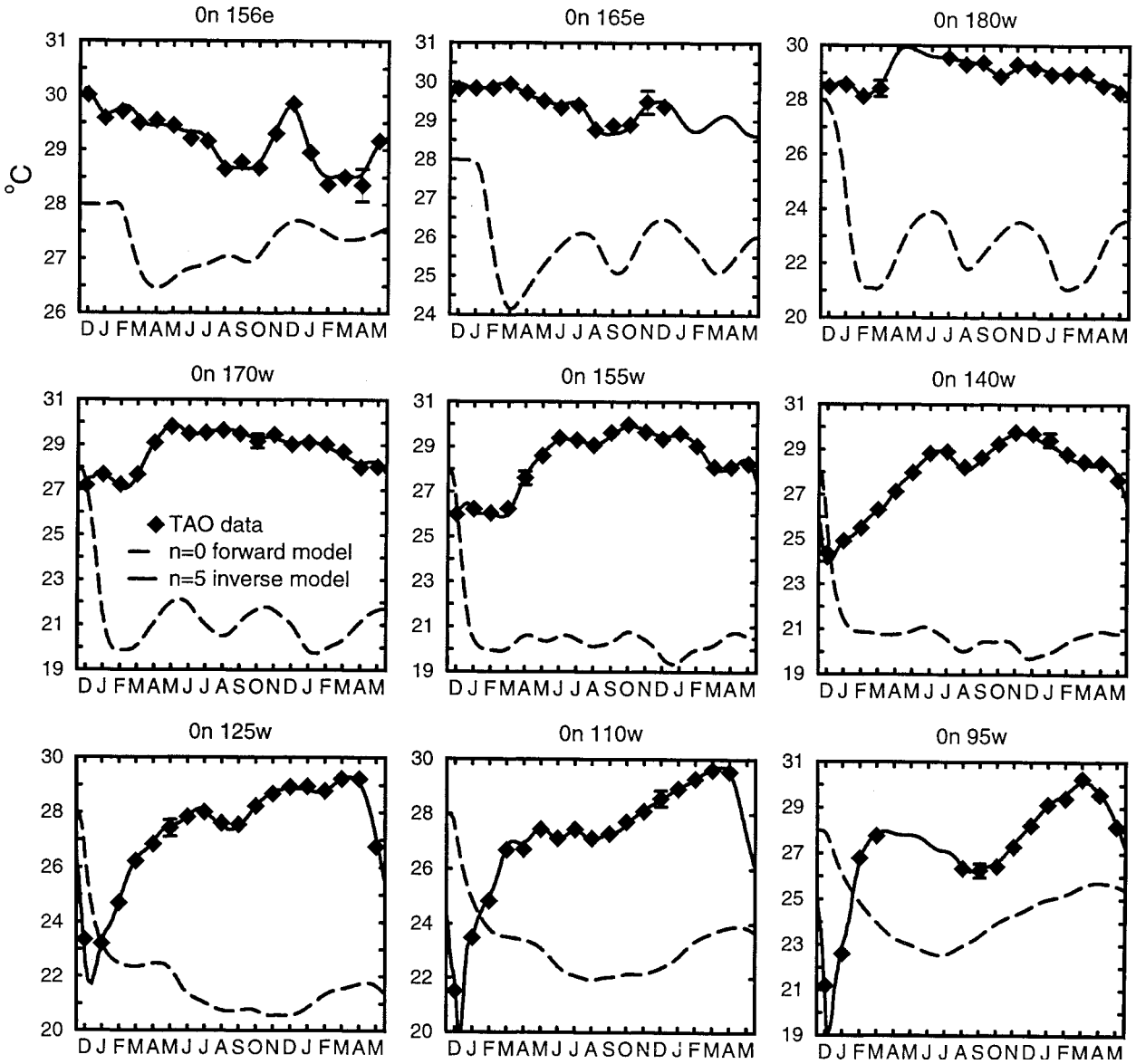

FIG. 7. SST time series at TAO buoys locations along the equator, from Dec 1996 to May 1998. The diamond symbols represent the data, the dashed line is the first background (model run without data, $n = 0$), and the solid line is the generalized inverse after five iterations. The error bar (0.3°C) is the same in each panel and for each data.

therm depth data failed as the lower-layer thickness always vanished during the first iteration on the nonlinearities.

6. Cross validation

Cross validation is the comparison of an inverse solution to independent data not used in the inversion. For the tropical Pacific and TAO data, the independant data here are measured currents and subsurface temperatures or isothermal layer depths, since we are assimilating only SST data. On one hand, the comparison with measured velocities is not reasonable when the model is subject to climatological wind forcing. However, such a comparison (not carried out here) is reasonable for an inverse solution computed with a reanalysis or real wind forcing. On the other hand, thickness data are, in general, estimated from the vertical temperature structure. Thus, cross validation by thickness data is an implicit cross validation by subsurface temperatures. Our solution cannot be so cross validated because of the poor vertical resolution and poor empirical parameterizations (fluxes, entrainment). The 2½-layer model allows us to estimate temperatures only at two vertical grid points (for each horizontal grid point). The resulting two-point vertical interpolation cannot produce a realistic map of

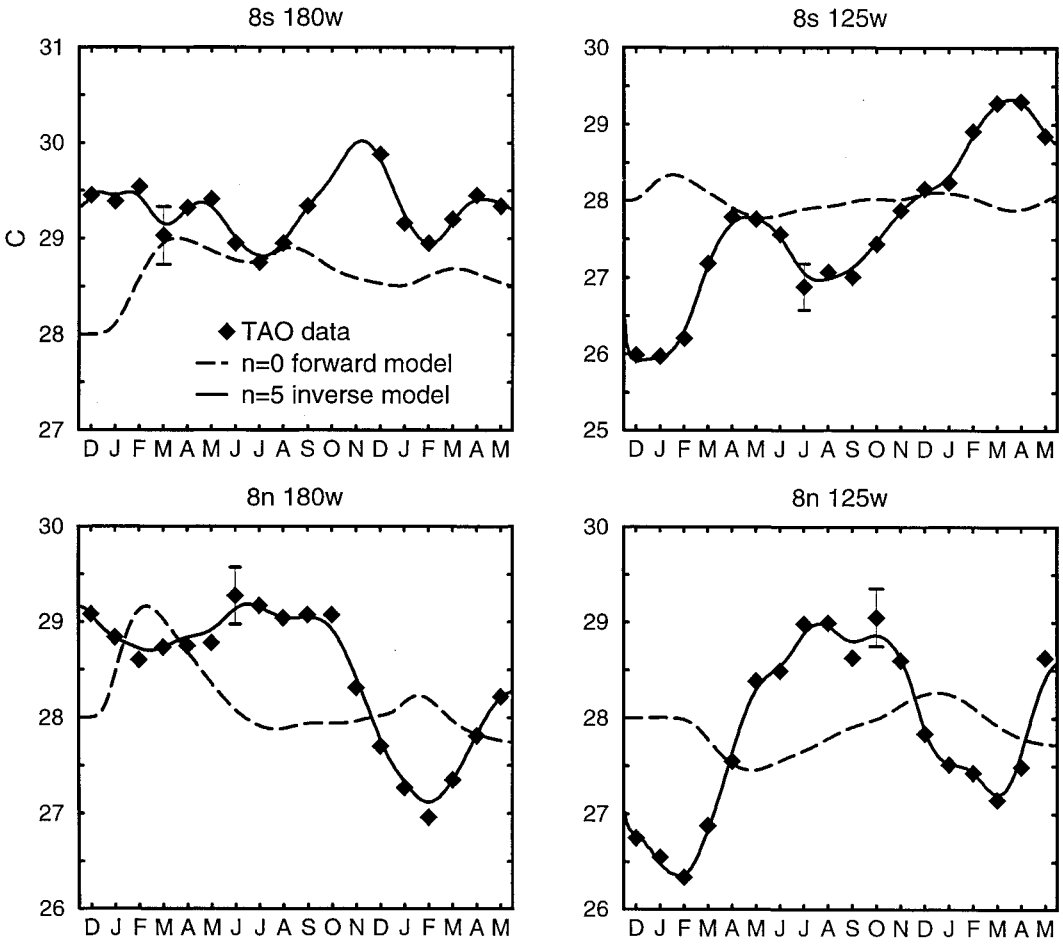

FIG. 8. Same as in Fig. 7 except for some locations off the equator.

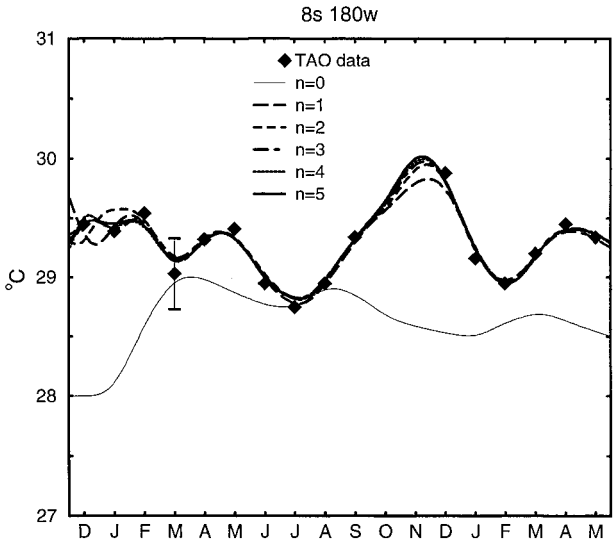

FIG. 9. Convergence of iterated SST time series from the generalized inversion at (8°S, 180°): data (diamonds), $n = 0$ (thin line), $n = 1$ (long-dashed line), $n = 2$ (dashed line), $n = 3$ (dotted–dashed line), $n = 4$ (dotted line), and $n = 5$ (solid line).

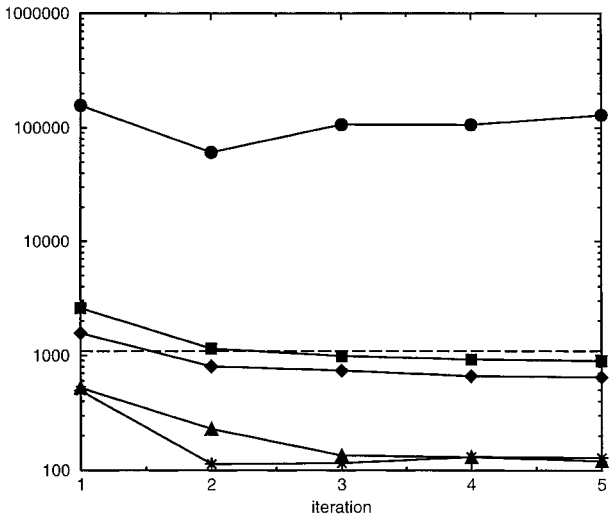

FIG. 10. Prior and posterior misfits with respect to iterations, and contributions to the posterior misfits: prior misfits (bullets), posterior misfits (squares), expected posterior misfits (dashed line), posterior dynamical misfits (diamonds), posterior data misfits (triangles), and posterior initial misfits (stars).

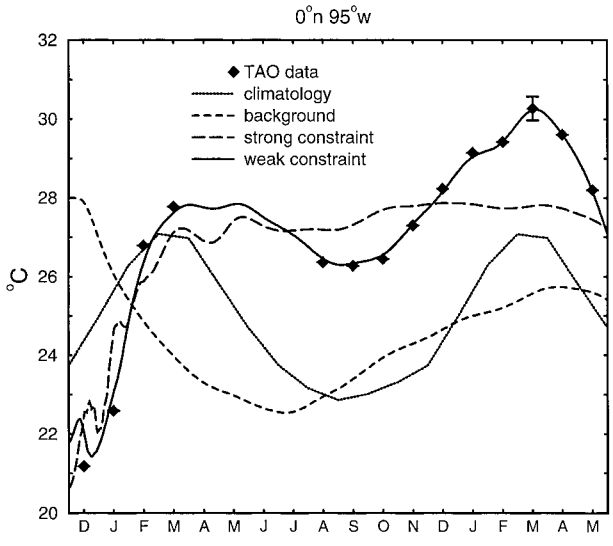

FIG. 11. Comparison between weak (solid line) and strong constraint (long-dashed line) experiments, the background (dashed line), the climatology (dotted line), and the data (diamonds), at (0°, 95°W).

the verical temperature structure. We are confronted here with the difficulty that the model is not designed to resolve the vertical temperature structure. Therefore, the cross validation here is limited to comparison with withheld SST data, that is, SST data that are not assimilated.

Keeping the same climatological wind forcing, we performed a second inversion in which we withheld SST data at eight different TAO mooring locations—(8°S, 170°W), (2°S, 155°W), (2°S, 110°W), (0°, 180°), (2°N, 125°W), (2°N, 95°W), (5°N, 165°W), and (8°N, 155°W)—for the whole time window of assimilation. The withheld data consist of 133 measurements (about 12%) out of the original set of 1088 data points. The resulting inverse solution is compared with the inverse solution including all SST data. First, we compare these inverse solutions at mooring locations where data are used in both inversions. As one would expect, both inverses fit the data very well: see Fig. 12. This also shows that the withheld data do not have impact on the fit to the remainder. Then we compare both inverses at mooring locations where data are withheld. Figure 13 shows

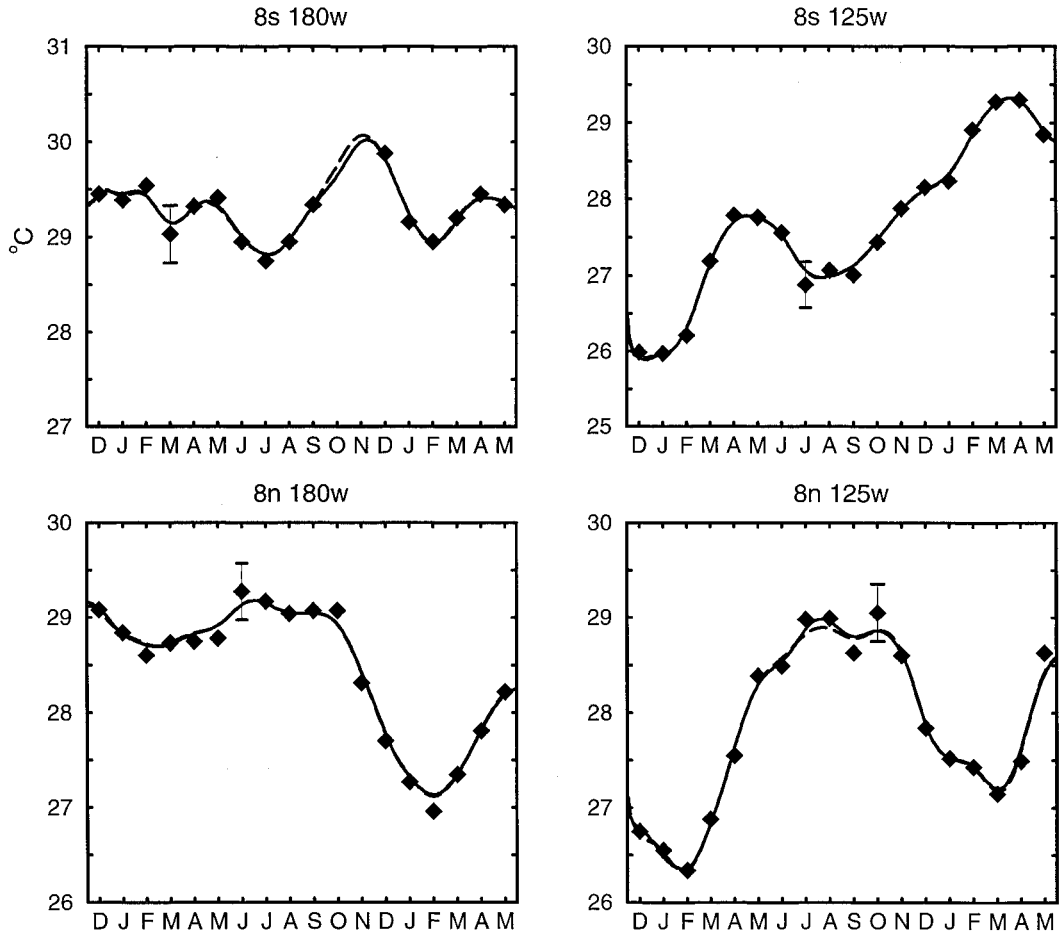

FIG. 12. Comparison between the inverse with all data (solid line) and the inverse with withheld data (long-dashed line) at locations where data are assimilated in both inverses.

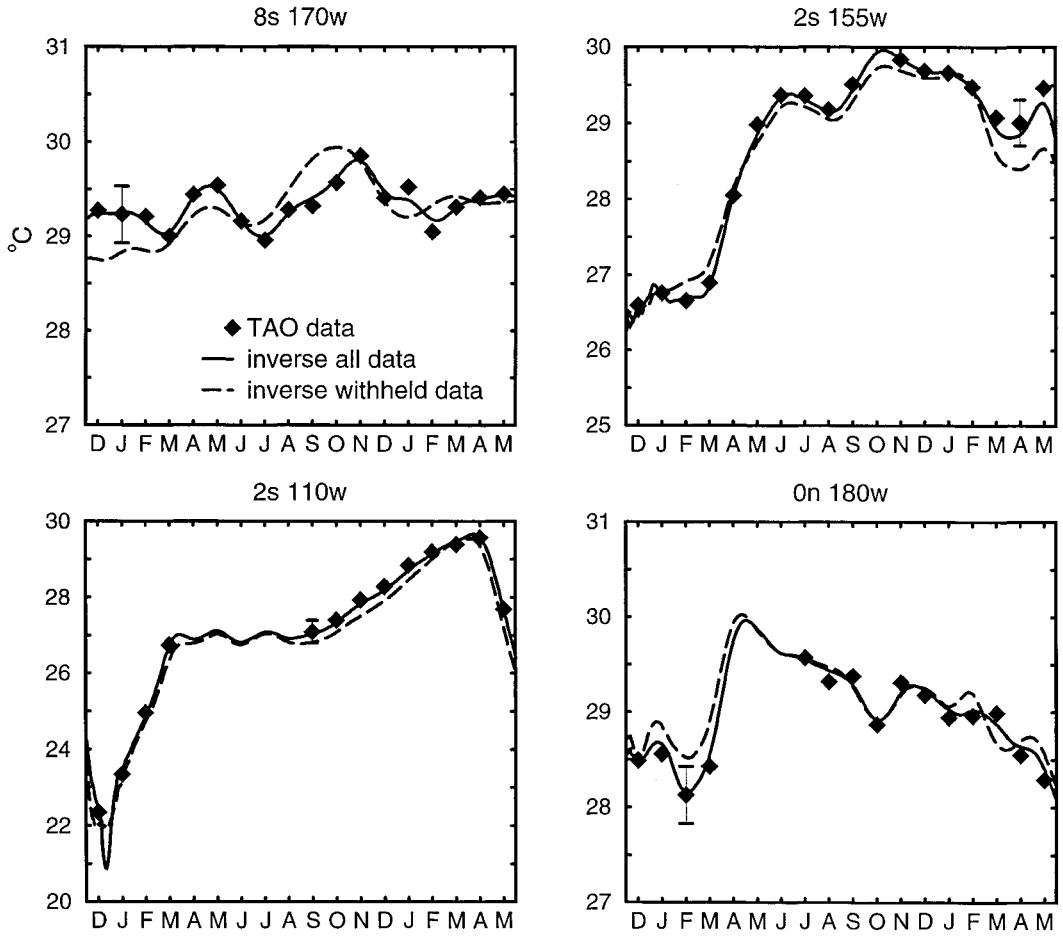

FIG. 13. Comparison between the inverse with all data (solid line) and the inverse with withheld data (long-dashed line) at locations where data are not assimilated in the second inversion.

that the second inverse (dashed line) compares very well with the first inverse (solid line). The former fits the withheld data to within one standard data error and remains close to the latter at the locations where data were withheld. However, the former occasionally misfits the data and strays from the first inverse (with all data) by slightly more than one standard error, but never exceeding 1.5 standard errors. This is the case, for example, from December 1996 to February 1997 and September to October 1997 at (8°S, 170°W), April to May 1998 at (2°S, 155°W), and February 1997 at (0°, 180°). Recall that the second inverse in Fig. 13 (dashed line) is independent of the data at the locations displayed. For conciseness, we do not present the total SST and SST anomaly maps from the second experiment, but they also show very good agreement with the first inverse, and hence with PMEL/TAO maps. Our second inverse solution thus survives this cross validation.

7. Real winds

We have computed a third inverse solution by replacing the climatological wind forcing with the FSU wind analyses for our period of interest. The winds were downloaded from the FSU wind products ftp site via the Internet. In this experiment, all the 1088 SST monthly mean data points are included in the inversion.

The monthly mean SST and SST anomaly maps from the inversion with FSU winds are shown in Fig. 14 for August 1997. This figure is to be compared with Fig. 5a. This new inverse solution reproduced the 4°–4.5°C anomalous warm pool in the eastern Pacific, which is consistent with the PMEL maps and in good agreement with the first inverse (forced by climatological winds). Both inverse maps are very similar for large-scale features. However, the third inverse, with real winds, displays more variability than the first inverse with climatological winds. The latter is smoother. This is not surprising, since the FSU winds are monthly mean wind fields based on real wind observations in the tropical Pacific for the period of time we are assimilating the data. Both inverses fit the data to within one standard error, as shown in Figs. 15 (off the equator) and 16 (along the equator). These time series plots confirm the remark that the inverse forced with FSU winds has more variability than the other.

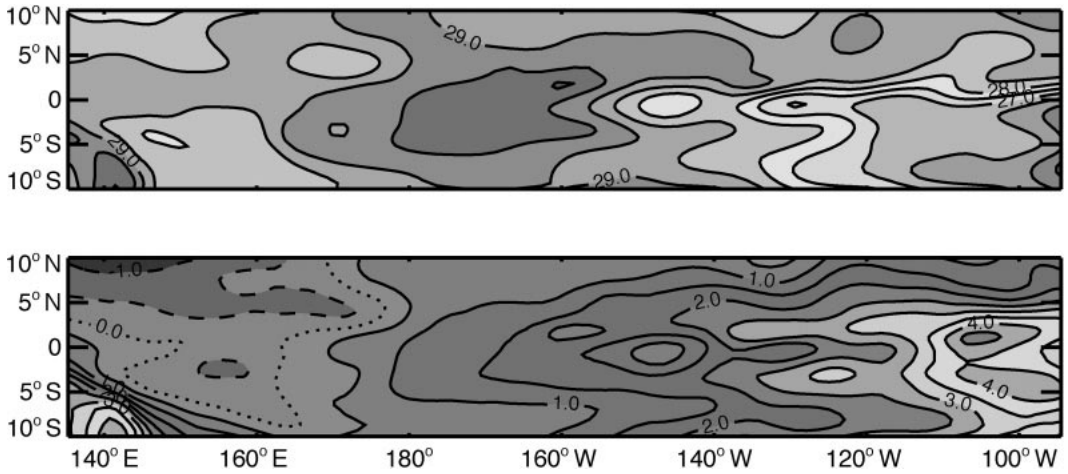

FIG. 14. Monthly means SST and SST anomalies from the generalized inverse with FSU winds for Aug 1997.

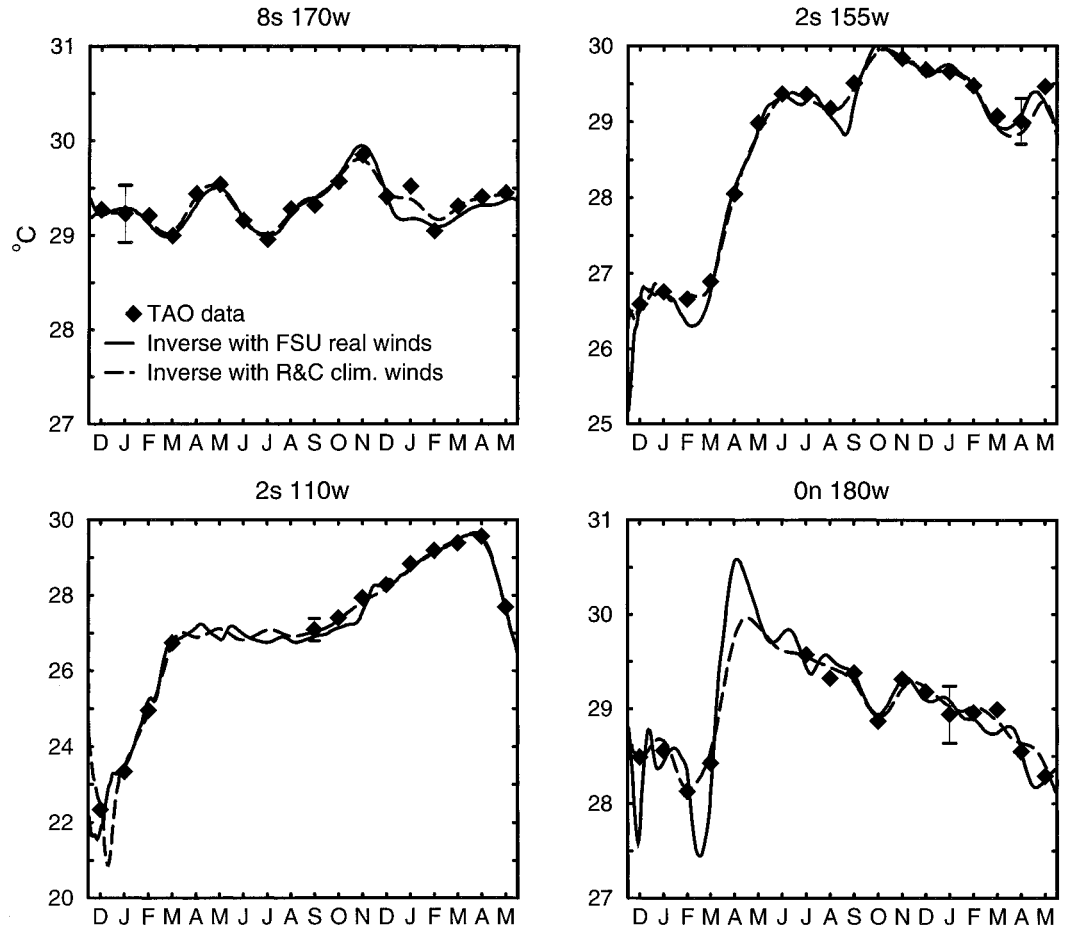

FIG. 15. Comparison between the inverse forced with FSU winds (solid line) and the inverse forced with climatological winds (long-dashed line) at some mooring locations.

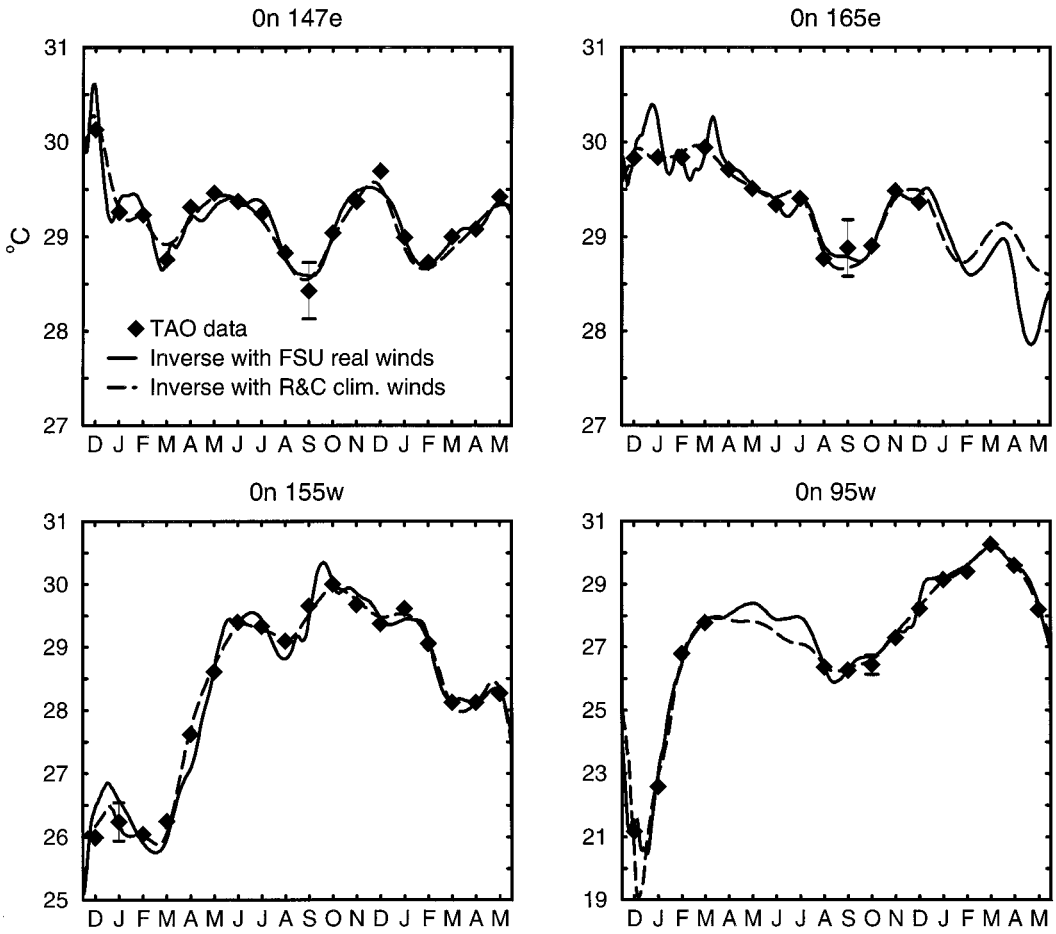

FIG. 16. Same as in Fig. 15 but all locations are along the equator.

What then, do we learn from these two experiments, since both inverses do fit the data to within one standard data error? Fitting the data is to achieve only one objective of data assimilation. Another equally important objective is the estimation of model errors, which include forcing errors. The two assumed wind forcings are erroneous first guesses of the ''true'' forcing, and we would like to ''invert'' the SST data in order to correct the first guesses. In Figs. 17 and 18, for the first and third inverses, respectively, we present (a) the first-guess wind fields, (b) the corrections estimated by the respective inverses, (c) and the corrected (first guess plus correction) winds. The month is December 1997, when the latest ENSO peaked. As one would expect, these figures clearly show that the climatological winds needed larger-amplitude corrections than do the FSU winds. At some places, the estimated corrections to the climatological wind exceed two standard deviations (0.05 N m^{-2}, as specified in section 3d). None that all the arrows in Figs. 17 and 18 are scaled by 0.25 N m^{-2} (longest arrow). Figure 17b shows that the inverse could detect westerly anomalous winds (near the equator, from the date line to about 115°W) by assimilating only SST data. The uncorrected and corrected FSU winds (Fig. 18c) are substantially stronger than the corrected climatological winds (Fig. 17c), which explains the difference in variability on the time series and maps as noted above.

All the results shown for the third inversion were obtained after two iterations. The inverse calculation had to be halted prior to convergence, as the upper layers in successive background fields were close to outcropping. We are discouraged from further work with layered models, and will work with sigma-coordinate-type models in the future.

8. Summary and conclusions

We have now advanced from the inverse of an intermediate coupled model (Bennett et al. 1998) to the inverse of a full nonlinear PE ocean model. The PE model is a 2½-layer reduced-gravity version, after McCreary and Yu (1992). We slightly modified their entrainment/detrainment formula and their treatment of vertical divergence terms, for Gâteaux differentiability. An iterated indirect representer method was then applied

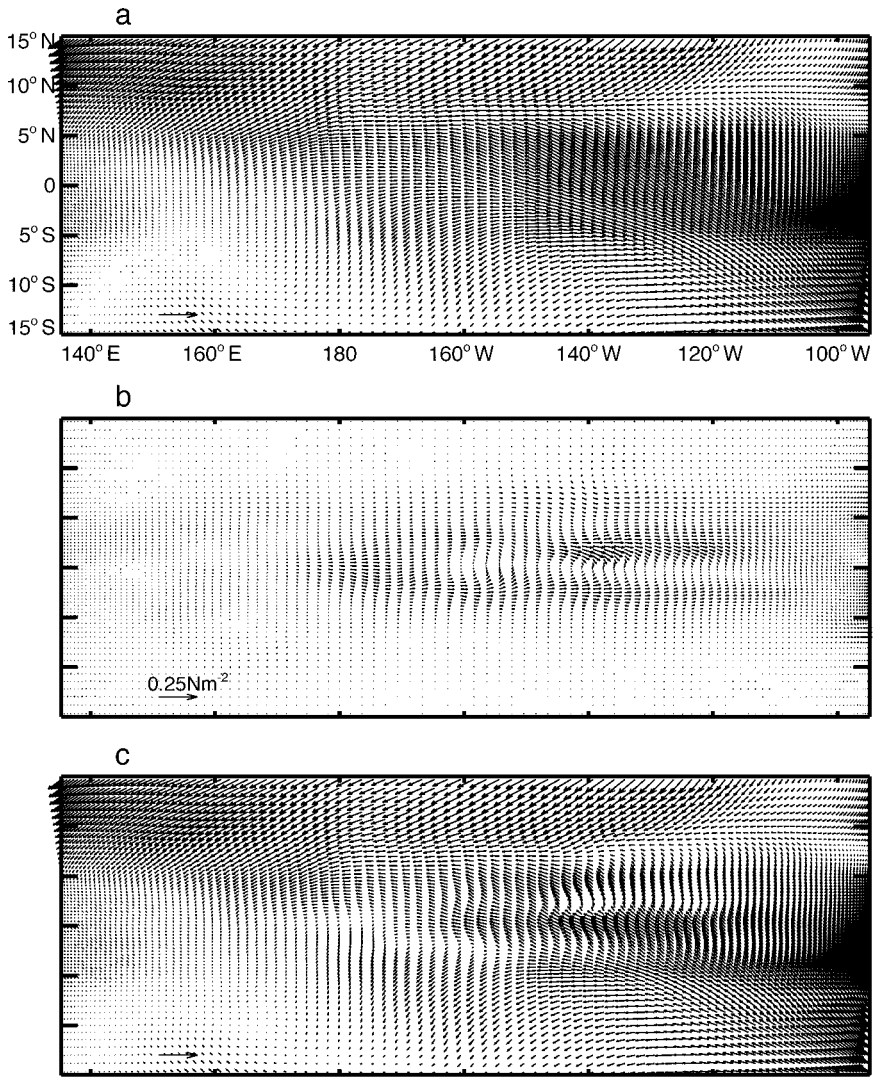

FIG. 17. Wind fields: (a) first guess from climatology, (b) correction estimated by the inverse, and (c) corrected first guess for Dec 1997.

to solve the nonlinear EL system (Bennett et al. 1996, 1998). We used a revised linearization of the EL system and thus avoided the computation and the storage of a first-guess field for the time-dependant adjoint variables.

Before solving an inverse model involving TAO data, we solved the nonlinear PE model iteratively. This is equivalent to an inversion without data. Starting from a first guess, each iterate was computed by tangent linearizing the model equations about the previous iterate. With smoothing relaxation, effective convergence was obtained after 30 iterations.

For the generalized inversion including data, the variances, length scales, and timescales for the model error covariances were estimated from observations of upper ocean eddy fluxes. We assumed that the parameterizations of the vertical fluxes of heat, momentum, and thickness in the model were 100% in error. We computed an inverse of the PE model, and 18 months of monthly mean TAO SST data from December 1996 to May 1998 covering the latest strong El Niño disturbance. The data were assimilated only at the mooring locations. The generalized inverse is in good agreement with the TAO project quick-look maps of the SST fields and anomalies. The inverse fits the data to within one standard data error and corrects discrepancies as large as 6° and 8°C between the very first background ($n = 0$) and the data at some mooring locations. The reduced penalty functional was about four standard deviations below the expected value. This indicates that we were pessimistic in our hypothesis about the means and covariances of the initial, model, and data errors. However, the reduced penalty functional $\hat{J}$ was only 17% smaller than the mean. Thus, rescaling all the prior variances uniformly by 17% would yield identically the same inverse (an extremum for J is an extremum for $2J$), but then the posterior penalty functional would be exactly equal to

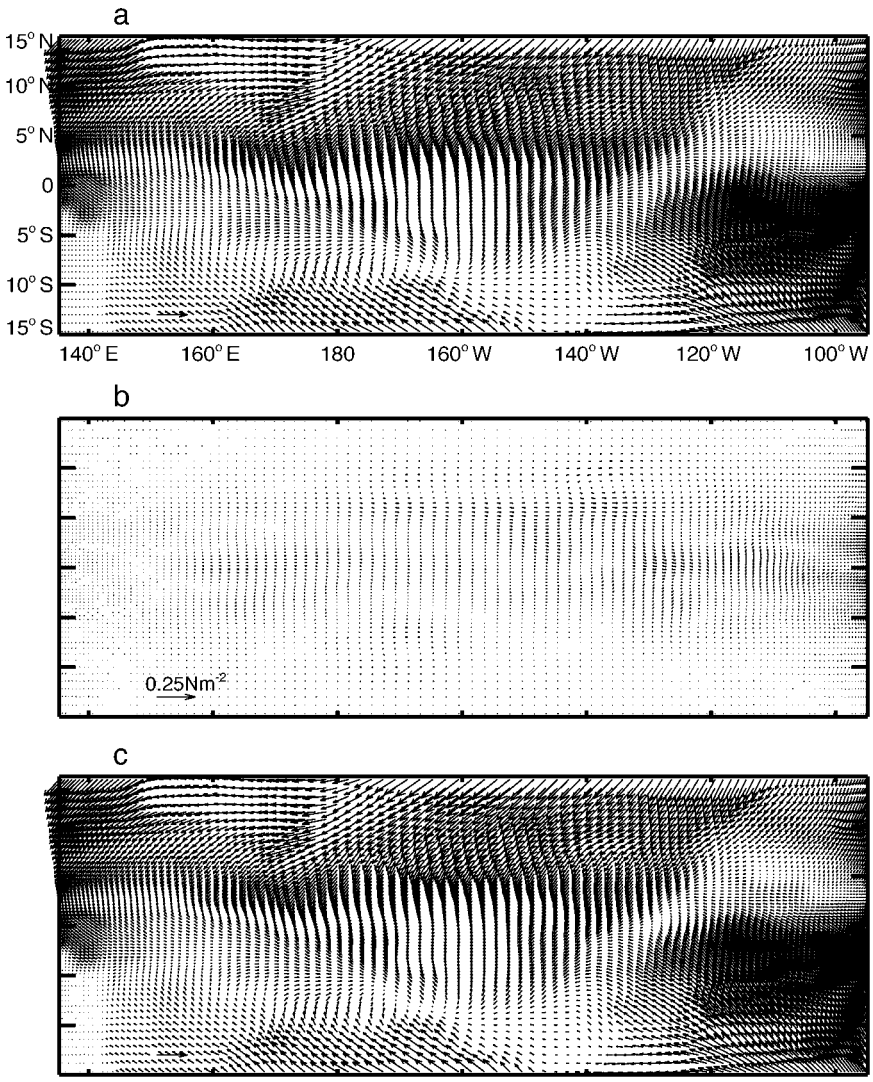

FIG. 18. Wind fields: (a) first guess from FSU, (b) correction estimated by the inverse, and (c) corrected first guess for Dec 1997.

its expected value of $M = 1088$. Such a minor rescaling of the prior variances yields values that are just as plausible as the original values. We conclude that the original hypothesis for the model errors, initial errors, and the data errors sensibly survives the significance test.

A small number of iterations (five) is needed for the inverses to converge, because the data ''guide'' the iterations.

The ''strong constraint'' inverse lost track of the data after about three months. However, a careful comparison between ''weak'' and ''strong'' constraint inverses should be made for a three-month inversion.

Guided by our experience when attempting to assimilate thickness data, and guided by the unconvincing representation of thickness in our low-resolution model, we do not expect it to cross validate well against thickness data. We have made no attempt to do so. Withholding 12% of the data did not prevent the inverse from fitting all SST data to within within one standard error, even at those mooring locations where the data were withheld. The first inverse was able to infer anomalous westerly winds. The TAO data were also inverted to find errors in FSU real-time winds. As expected, the error estimates were smaller than those for the climatological winds, but the inverse calculation had to be halted prior to convergence, as the upper layer in successive background fields was close to an outcropping. Again, we are discouraged from further work with layered models and will work with sigma-coordinate-type models in the future.

Because of the poor vertical resolution of the model, we were limited to the assimilation of SST data only. Future work will include an ocean model with finer vertical resolution, specifically a 15½-level sigma-co-

ordinate reduced-gravity PE modeled closely after Gent and Cane (1989). It will be inverted with surface and subsurface TAO data.

Acknowledgments. This work is supported by NSF 9520956-OCE and by ONR N00014-93-1-0422. All the computations were performed on the COAS CM-5 and CM-500e systems. The COAS CM-5 is supported by NASA EOS, and we are grateful to Mark Abbott for access to it. The COAS CM-500e systems were donated by the Office of Naval Research. The TAO data were kindly prepared and provided by Dai McClurg of NOAA/PMEL. The authors would like to thank D. Ed Harrison and J. McPhaden of NOAA/PMEL for constructive collaboration and helpful discussions. The FSU winds are available through the Internet from the ftp site ftp://coaps.fsu.edu/pub/wind/pac/.

APPENDIX

Linearization

Here we describe the slight modifications mentioned in section 2 and the detailed linearization of all the nonlinearities appearing in the PE model (1)–(9), by applying the linearization scheme described in (23).

Three types of nonlinearities are present in the model: products (basically found in the nonlinear advection and the pressure gradients), divisions (by layer thicknesses obtained when deriving the advective form of the model), and switches (in the entrainment/detrainment formulas).

(i) The products: for any two model variables U and V, the product UV is symmetrically linearized following (23) as

$$(UV)^n = U^{n-1}V^n + (U^n - U^{n-1})V^{n-1}, \quad \text{(A1)}$$

where the superscript n is the iteration index. The principle remains the same when a linear operator acts on U or V or on the product.

(ii) The divisions: also following (23), the ratio U/V is linearized as

$$\left(\frac{U}{V}\right)^n = \frac{U^n}{V^{n-1}} - \frac{U^{n-1}(V^n - V^{n-1})}{(V^{n-1})^2}, \quad \text{(A2)}$$

provided that V^{n-1} does not vanish.

(iii) The entrainment: the linearization of the entrainment/detrainment presents two major difficulties, as the formula uses switches (the Heaviside functions) and is quadratic. We want to rewrite the entrainment as a linear functional of h_1^n. We linearize these formulas in two steps. First, we use one expression for entrainment, in order to avoid the discontinuities introduced by the Heaviside functions in (6) and (7). The sign of the new entrainment should change as indicated by the Heaviside functions. Therefore, we replaced (6) and (7) by

$$w = \frac{(H_e - h_1)^3}{H_e^2 t_e}. \quad \text{(A3)}$$

The second step consists of replacing the first-order upwind scheme used by McCreary and Yu (1992) in the discretization of the vertical advection terms. We define the momentum and temperature at the interface to be the mean of their respective values in the upper and the lower layers, which is commonly used in layer models. For example, the temperature at the interface is defined as $(T_1 + T_2)/2$ (Gent and Cane 1989; Murtugudde et al. 1995), instead of T_1 or T_2 depending on the sign of the entrainment, since checking the sign of the entrainment is a nonlinear operation. The vertical advection terms then become sums of products of the model variables that we can linearize as described above.

The full linearized equations of the forward model are

$$\frac{\partial \mathbf{v}_i^n}{\partial t} + \mathbf{v}_i^{n-1}\cdot\boldsymbol{\nabla}\mathbf{v}_i^n + (\mathbf{v}_i^n - \mathbf{v}_i^{n-1})\cdot\boldsymbol{\nabla}\mathbf{v}_i^{n-1} + f\mathbf{k}\times\mathbf{v}_i^n + \boldsymbol{\nabla}p_i^n$$

$$= \delta_{1_i}\left(\frac{\boldsymbol{\tau}}{h_1^{n-1}} - \frac{\boldsymbol{\tau}(h_1^n - h_1^{n-1})}{(h_1^{n-1})^2}\right) + \frac{[w^{n-1}(\mathbf{v}_1^n - \mathbf{v}_2^n) + (w^n - w^{n-1})(\mathbf{v}_1^{n-1} - \mathbf{v}_2^{n-1})]}{2h_i^{n-1}} - \frac{w^{n-1}}{2}(\mathbf{v}_1^{n-1} - \mathbf{v}_2^{n-1})\frac{(h_i^n - h_i^{n-1})}{(h_i^{n-1})^2}$$

$$+ \kappa_2\nabla^2\mathbf{v}_i^n - \gamma\mathbf{i}u_i^n + r_{\mathbf{v}_i}^n + \nu\nabla^2(\mathbf{v}_i^n - \mathbf{v}_i^{n-1}), \quad \text{(A4)}$$

$$\frac{\partial T_i^n}{\partial t} + \mathbf{v}_i^{n-1}\cdot\boldsymbol{\nabla}T_i^n + (\mathbf{v}_i^n - \mathbf{v}_i^{n-1})\cdot\boldsymbol{\nabla}T_i^{n-1}$$

$$= \frac{Q_i^n}{h_i^{n-1}} - \frac{Q^{n-1}(h_i^n - h_i^{n-1})}{(h_i^{n-1})^2} + \frac{[w^{n-1}(T_1^n - T_2^n) + (w^n - w^{n-1})(T_1^{n-1} - T_2^{n-1})]}{2h_i^{n-1}} - \frac{w^{n-1}}{2}(T_1^{n-1} - T_2^{n-1})\frac{(h_i^n - h_i^{n-1})}{(h_i^{n-1})^2}$$

$$+ \kappa_2\nabla^2 T_i^n + r_{T_i}^n + \nu\nabla^2(T_i^n - T_i^{n-1}), \quad \text{(A5)}$$

$$\frac{\partial h_i^n}{\partial t} + \boldsymbol{\nabla}\cdot[h_i^{n-1}\mathbf{v}_i^n + (h_i^n - h_i^{n-1})\mathbf{v}_i^{n-1}] = w^n + \kappa_2\nabla^2 h_i^n + r_{h_i}^n + \nu\nabla^2(h_i^n - h_i^{n-1}), \quad \text{(A6)}$$

where $r^n_{\mathbf{v}_i}$, $r^n_{T_i}$, and $r^n_{h_i}$ are the residuals for the momentum, temperature, and layer thicknesses. All the iterations are subject to the same initial and boundary conditions:

- initial conditions,

$$\mathbf{v}_i^n = 0, \qquad T_i^n = T_i^*, \qquad h_i^n = H_i, \quad \text{at } t = 0;$$

- north and south,

$$\frac{\partial u^n}{\partial y} = v^n = \frac{\partial h^n}{\partial y} = \frac{\partial T^n}{\partial y} = 0;$$

- east and west,

$$u^n = v^n = \frac{\partial h^n}{\partial x} = \frac{\partial T^n}{\partial x} = 0.$$

The linearized pressure gradient, entrainment, and heat fluxes terms are given by

$$\begin{aligned}\nabla p_1^n = {} & \alpha g \nabla [h_1^{n-1}(T_1^n - T_3) + (h_1^n - h_1^{n-1})(T_1^{n-1} - T_3) \\ & + h_2^{n-1}(T_2^n - T_3) + (h_2^n - h_2^{n-1})(T_2^{n-1} - T_3)] \\ & - \frac{1}{2}\alpha g [h_1^{n-1}\nabla T_1^n + (h_1^n - h_1^{n-1})\nabla T_1^{n-1}], \end{aligned} \tag{A7}$$

$$\begin{aligned}\nabla p_2^n = {} & \alpha g \nabla [(h_1^{n-1} + h_2^{n-1})(T_2^n - T_3) \\ & + (h_1^n + h_2^n - h_1^{n-1} - h_2^{n-1})(T_2^{n-1} - T_3)] \\ & - \alpha g \left[\left(h_1^{n-1} + \frac{h_2^{n-1}}{2} \right) \nabla T_2^n \right. \\ & \left. + \left(h_1^n + \frac{h_2^n}{2} - h_1^{n-1} - \frac{h_2^{n-1}}{2} \right) \nabla T_2^{n-1} \right], \end{aligned} \tag{A8}$$

$$w^n = 3\frac{(H_e - h_1^{n-1})^2(H_e - h_1^n)}{H_e^2 t_e} - 2\frac{(H_e - h_1^{n-1})^3}{H_e^2 t_e}, \tag{A9}$$

$$Q_1^n = \frac{H_1}{t_1}(T_1^* - T_1^n), \quad \text{and} \tag{A10}$$

$$Q_2^n = \frac{H_2}{t_2}(T_2^* - T_2^n), \tag{A11}$$

where α, g, H_e, H_1, H_2, t_e, t_1, t_2, T_1^*, T_2^*, and T_3 are constants.

The penalty functional we minimize at each iterate is

$$\begin{aligned} J^n = {} & J^n[u^n, v^n, T^n, h^n] \\ = {} & \sum_{i=1}^{2} r^n_{u_i} \bullet W_{u_i} \bullet r^n_{u_i} + r^n_{v_i} \bullet W_{v_i} \bullet r^n_{v_i} + r^n_{T_i} \bullet W_{T_i} \bullet r^n_{T_i} \\ & + r^n_{h_i} \bullet W_{h_i} \bullet r^n_{h_i} + \text{initial misfits} + \text{data misfits}. \end{aligned} \tag{A12}$$

We did not include boundary misfits in this experiment. The weights in the penalty functional are the inverses of prior estimates of covariances of respective dynamical residuals. In practice, we do not need to invert these covariances. The minimization algorithm can be formulated with the covariances only, see Bennett (1992). The • symbols in (36) denote integrals over space and time such as

$$\begin{aligned} & r^n_{u_i} \bullet W_{u_i} \bullet r^n_{u_i} \\ & = \int_0^T dt \int_0^T dt' \int_0^L dx \int_0^L dy \int_0^L dx' \int_0^L dy' r^n_{u_i} \\ & \quad \times (x, y, t) W_{u_i}(x, y, t, x', y', t') r^n_{u_i}(x', y', t'). \end{aligned} \tag{A13}$$

We chose not to include the adjoint equations in the paper, since they are readily (if tediously) derived from the linearized forward model as described in section 3b.

REFERENCES

Bennett, A. F., 1992: *Inverse Methods in Physical Oceanography*. Cambridge University Press, 346 pp.

——, and M. A. Thorburn, 1992: The generalized inverse of a nonlinear quasi-geostrophic ocean circulation model. *J. Phys. Oceanogr.*, **22,** 213–230.

——, B. S. Chua, and L. M. Leslie, 1996: Generalized inversion of a global numerical weather prediction model. *Meteor. Atmos. Phys.*, **60,** 165–178.

——, ——, D. E. Harrison, and M. J. McPhaden, 1998: Generalized inversion of Tropical Atmosphere–Ocean data and a coupled model of the tropical Pacific. *J. Climate,* **11,** 1768–1792.

Gent, P. R., and M. Cane, 1989: A reduced gravity, primitive equation model of the upper equatorial ocean. *J. Comput. Phys.*, **81,** 444–480.

Hagelberg, C. A., A. F. Bennett, and D. A. Jones, 1996: Local existence results for the generalized inverse of the vorticity equation in the plane. *Inverse Probl.*, **12,** 437–454.

Lacarra, J. F., and O. Talagrand, 1988: Short-range evolution of small perturbations in a barotropic model. *Tellus,* **40A,** 81–95.

McCreary, J. P., and Z. Yu, 1992: Equatorial dynamics in a 2½-layer model. *Progress in Oceanography,* Vol. 29, Pergamon Press, 61–132.

Milne, R. D., 1980: *Applied Functional Analysis: An Introductory Treatment.* Pitman Publishing, 289 pp.

Moum, J. N., 1996: Energy-containing scales of turbulence in the ocean thermocline. *J. Geophys. Res.*, **101** (C6), 14 095–14 109.

——, D. R. Caldwell, and C. A. Paulson, 1989: Mixing in the equatorial surface layer and thermocline. *J. Geophys. Res.*, **94** (C2), 2005–2021.

Murtugudde, R., M., Cane, and V. Prasad, 1995: A reduced gravity, primitive equation, isopycnal ocean GCM: Formulation and simulations. *Mon. Wea. Rev.*, **123,** 2864–2887.

Peters, H., 1994: The diurnal cycle of the upper ocean: Turbulence, fine-scale shear, and mean shear. *J. Geophys. Res.*, **99** (C4), 7707–7723.

——, M. C. Gregg, and J. M. Toole, 1988: On the parameterization of the equatorial turbulence. *J. Geophys. Res.*, **93** (C2), 1199–1218.

——, ——, and T. B. Sanford, 1991: Equatorial and off-equatorial fine-scale and large-scale shear variability at 140W. *J. Geophys. Res.*, **96** (C9), 16 913–16 928.

Rasmusson, E. M., and T. H. Carpenter, 1982: Variations in tropical sea surface temperature and surface wind fields associated with the Southern Oscillation/El Niño. *Mon. Wea. Rev.*, **110,** 354–384.

Sasaki, Y., 1970: Some basic formalisms in numerical variational analysis. *Mon. Wea. Rev.*, **98,** 875–883.